

## CHAPTER 8

---

# THRUST CHAMBERS

---

The *thrust chamber* is the key subassembly of a rocket engine. Here the liquid propellants are metered, injected, atomized, vaporized, mixed, and burned to form hot reaction gas products, which in turn are accelerated and ejected at high velocity (see Refs. 6-1 and 6-2). This chapter describes thrust chambers, their components, cooling, ignition, and heat transfer. A rocket thrust chamber assembly (Figs. 8-1 and 8-2) has an *injector*, a *combustion chamber*, a *supersonic nozzle*, and *mounting provisions*. All have to withstand the extreme heat of combustion and the various forces, including the transmission of the thrust force to the vehicle. There also is an ignition system if non-spontaneously ignitable propellants are used. Some thrust chamber assemblies also have integrally mounted propellant valves and sometimes a thrust vector control device, as described in Chapter 16. Table 8-1 (see pages 272-273) gives various data about five different thrust chambers with different kinds of propellants, cooling methods, injectors, feed systems, thrust levels, or nozzle expansions. Some engine parameters are also listed. Some of the terms used in this table will be explained later in this chapter.

The basic analyses for thrust chamber performance (specific impulse, combustion temperature) are given in Chapter 5, the basic design parameters (thrust, flow, chamber pressure, or throat area) are in Chapter 3, and the combustion phenomena in Chapter 9.

Although we use the word *thrust chamber* in this book (for rocket engines generally larger than 1000 lbf thrust), some articles use the term *thrust cylinder* or *rocket combustor*. We will also use the term *thruster* for small thrust units, such as attitude control thrusters, and for electrical propulsion systems.

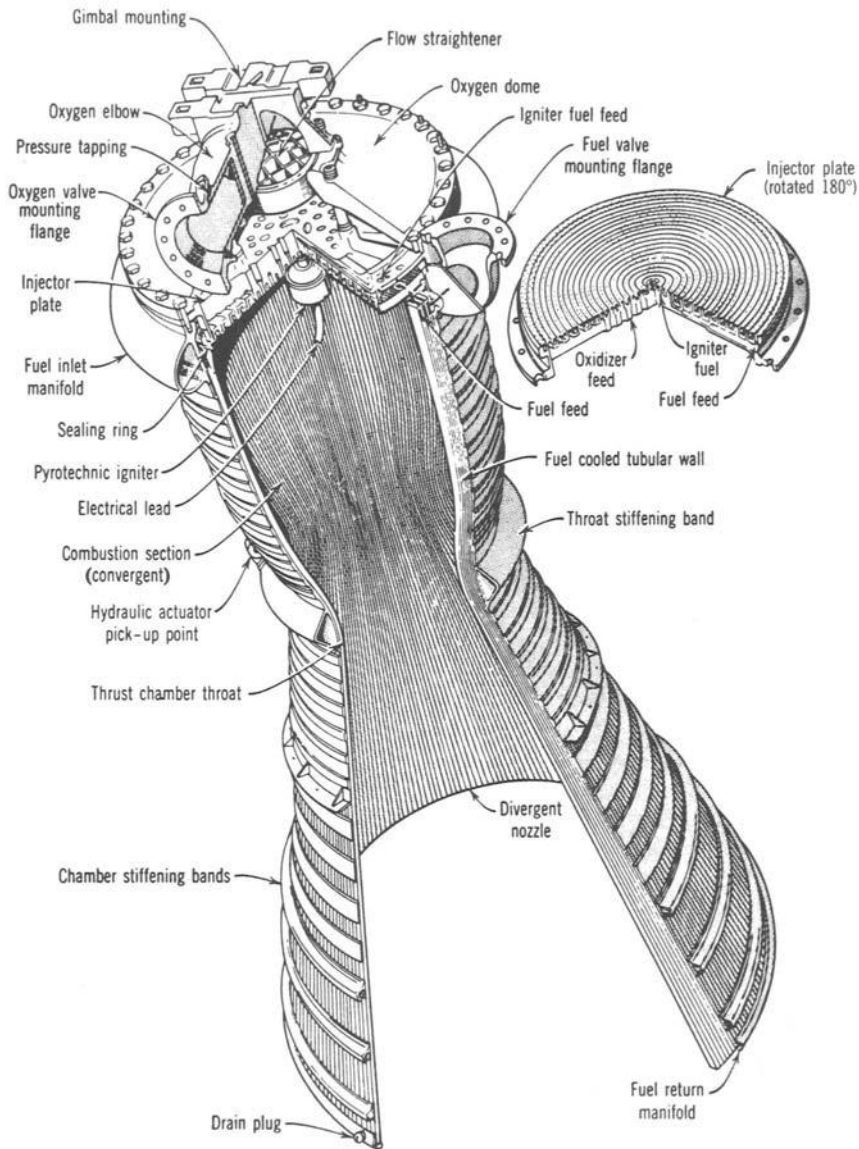


**FIGURE 8-1.** Construction of a regeneratively cooled tubular thrust chamber using a kerosene-type fuel and liquid oxygen, as originally used in the Thor missile. The nozzle inside diameter is about 15 in. The sea-level thrust was originally 120,000 lbf, but was uprated to 135,000, then 150,000, and finally to 165,000 lbf by increasing the flow and chamber pressure and strengthening and modifying the hardware. The cone-shaped exit cone was replaced by a bell-shaped nozzle. Figure 8-9 shows how the fuel flows down through every other tube and returns through the adjacent tube before flowing into the injector. Figure 8-4 shows the flow passages in a similar injector. (Courtesy of Rolls Royce, England.)

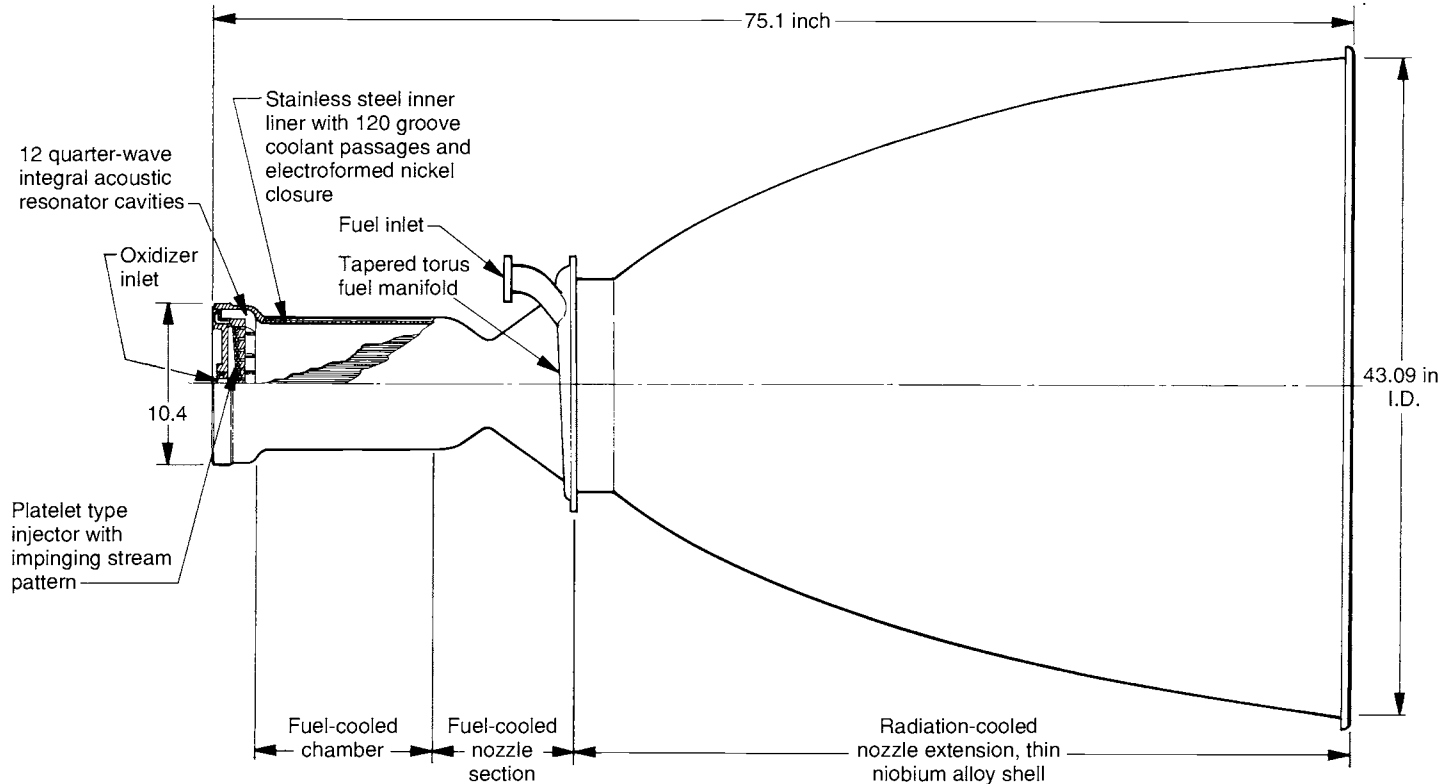


**FIGURE 8-2.** Simplified half-section of one of the two thrust chambers of the orbital maneuvering engines used on the Space Shuttle vehicle. Each develops a vacuum thrust of 6000 lbf (26,689 N) and delivers a minimum vacuum specific impulse of 310 sec, using nitrogen tetroxide and monomethyl hydrazine propellants at a nominal mixture ratio of 1.65 and a nominal chamber pressure of 128 psia. It is designed for 100 flight missions, a service life of 10 years, and a minimum of 500 starts. These engines provide the thrust for final orbit attainment, orbit circularization, orbit transfer, rendezvous, and deorbit maneuvers. The nozzle area ratio of 55:1. (Courtesy of Aerojet Propulsion Company.)

## 8.1. INJECTORS

The functions of the injector are similar to those of a carburetor of an internal combustion engine. The injector has to introduce and meter the flow of liquid propellants to the combustion chamber, cause the liquids to be broken up into small droplets (a process called atomization), and distribute and mix the propellants in such a manner that a correctly proportioned mixture of fuel and oxidizer will result, with uniform propellant mass flow and composition over the chamber cross section. This has been accomplished with different types of injector designs and elements; several common types are shown in Fig. 8-3 and complete injectors are shown in Figs. 9-6, 8-1, and 8-4.

The *injection hole pattern* on the face of the injector is closely related to the internal manifolds or feed passages within the injector. These provide for the distribution of the propellant from the injector inlet to all the injection holes. A large complex manifold volume allows low passage velocities and good distribution of flow over the cross section of the chamber. A small manifold volume allows for a lighter weight injector and reduces the amount of "dribble" flow after the main valves are shut. The higher passage velocities cause a more uneven flow through different identical injection holes and thus a poorer distribution and wider local gas composition variation. Dribbling results in afterburning, which is an inefficient irregular combustion that gives a little "cutoff" thrust after valve closing. For applications with very accurate terminal vehicle velocity requirements, the cutoff impulse has to be very small and reproducible and often valves are built into the injector to minimize passage volume.

*Impinging-stream-type, multiple-hole injectors* are commonly used with oxygen-hydrocarbon and storable propellants. For *unlike doublet* patterns the propellants are injected through a number of separate small holes in such a manner that the fuel and oxidizer streams impinge upon each other. Impingement forms thin liquid fans and aids atomization of the liquids into droplets, also aiding distribution. Characteristics of specific injector orifices are given in Table 8-2 (see page 279). Impinging hole injectors are also used for *like-on-like* or *self-impinging patterns* (fuel-on-fuel and oxidizer-on-oxidizer). The two liquid streams then form a fan which breaks up into droplets. Unlike doublets work best when the hole size (more exactly, the volume flow) of the fuel is about equal to that of the oxidizer and the ignition delay is long enough to allow the formation of fans. For uneven volume flow the triplet pattern seems to be more effective.

The *nonimpinging* or *shower head* injector employs nonimpinging streams of propellant usually emerging normal to the face of the injector. It relies on turbulence and diffusion to achieve mixing. The German World War II V-2 rocket used this type of injector. This type is now not used, because it requires a large chamber volume for good combustion. *Sheet* or *spray-type injectors* give cylindrical, conical, or other types of spray sheets; these sprays generally intersect and thereby promote mixing and atomization. By varying the width of the sheet (through an axially moveable sleeve) it is possible to throttle the propel-

TABLE 8-1. Thrust Chamber Characteristics

	Engine Designation				
	RL 10B-2	LE-7 (Japan)	RCS	RS-27	AJ-10-118I
Application	Delta-III and IV upper stage	Booster stage for H-II launcher	Attitude control	Delta II Space Launch booster	Delta II Second stage
Manufacturer	Pratt & Whitney, United Technologies Corporation	Mitsubishi Heavy Industries	Kaiser Marquardt Company	The Boeing Co., Rocketdyne Propulsion & Power	Aerojet Propulsion Company
<i>Thrust Chamber</i>					
Fuel	Liquid H <sub>2</sub>	Liquid H <sub>2</sub>	MMH	RP-1 (kerosene)	50% N <sub>2</sub> H <sub>4</sub> /50% UDMH
Oxidizer	Liquid O <sub>2</sub>	Liquid O <sub>2</sub>	N <sub>2</sub> O <sub>4</sub>	Liquid oxygen	N <sub>2</sub> O <sub>4</sub>
Thrust chamber thrust (lbf)					
at sea level (lbf)	No sea level firing	190,400	12	164,700	NA
in vacuum (lbf)	24,750	242,500	18	207,000	9850
Thrust chamber mixture ratio	5.88	6.0	2.0	2.35	1.90
Thrust chamber specific impulse					
at sea level (sec)	NA	349.9	200	257	
in vacuum (sec)	462	445.6	290	294	320
Characteristic exhaust velocity, $c^*$ (ft/sec)	7578	5594.8	5180	5540	5606
Thrust chamber propellant flow (lb/sec)	53.2	346.9	0.062	640	30.63
Injector end chamber pressure (psia)	640	—	70	576	125
Nozzle end stagnation pressure (psia)	NA	1917	68	534	
Thrust chamber sea level weight (lbf)	< 150	1560	7	730	137
Gimbal mount sea level weight (lbf)	< 10	57.3	NA	70	23
Chamber diameter (in.)	—	15.75	1.09	21	11.7
Nozzle throat diameter (in.)	5.2	9.25	0.427	16.2	7.5
Nozzle exit diameter (in.)	88	68.28	3.018	45.8	60
Nozzle exit area ratio	285	54:1	50:1	8:1	65:1

Chamber contraction area ratio	—	2.87	6:1	1.67:1	2.54:1
Characteristic chamber length $L^*$ (in.)	—	30.7	18	38.7	30.5
Thrust chamber overall length (in.)	90	14.8	11.0	86.15	18.7
Fuel jacket and manifold volume (ft <sup>3</sup> )	—	3.5	—	2.5	—
Nozzle extension	Carbon-carbon	None	None	None	None
Cumul. firing duration (sec)	> 360*	*	*	*	> 150
Restart capability	Yes	No	Yes	No	Yes
Cooling system	Stainless steel tubes, 1½ passes regenerative cooled	Regenerative (fuel) cooled, stainless steel tubes	Radiation cooled, niobium	Stainless steel tubes, single pass, regenerative cooling	Ablative layer is partly consumed
Tube diameter/channel width (in.)	NA	0.05 (channel)	NA	0.45	Ablative material: Silica phenolic
Number of tubes	NA	288	0	292	NA
Jacket pressure drop (psi)	253	540	NA	100	NA
Injector type	Concentric annular swirl and resonator cavities	Hollow post/sleeve elements; baffle and acoustic cavities	Drilled holes	Flat plate, drilled rings and baffle	Outer row: shower head; triplets & doublets, with dual tuned resonator
Injector pressure drop—oxidizer (psi)	100	704	50	156	40
Injector pressure drop—fuel (psi)	54	154	50	140	40
Number of oxidizer injector orifices	216	452 (coaxial)	1	1145	1050
Number of fuel injector orifices	216	452 (coaxial)	1	1530	1230

#### Engine Characteristics

Feed system	Turbopump with expander cycle	Turbopump	Pressure fed tanks	Turbopump with gas generator	Pressure fed tanks
Engine thrust (at sea level) (lb)	NA	190,400	12	165,000	NA
Engine thrust (altitude) (lb)	24,750	242,500	18	207,700	9850
Engine specific impulse at sea level	NA	349.9	200	253	320
Engine specific impulse at altitude	462	445.6	290	288	320
Engine mixture ratio (oxidizer/fuel)	5.88	6.0	2.0	2.27	1.90

\*limited only by available propellant.

Sources: Companies listed above and NASA.

The thrust for the thrust chamber is usually slightly less than the thrust of the engine for open cycles, such as a gas generator cycle; the thrust chamber specific impulse is actually slightly higher (about 1%) than the engine specific impulse. For closed cycles such as the staged combustion cycle, the  $F$  and  $I_s$  values of the engine and thrust chamber are the same.

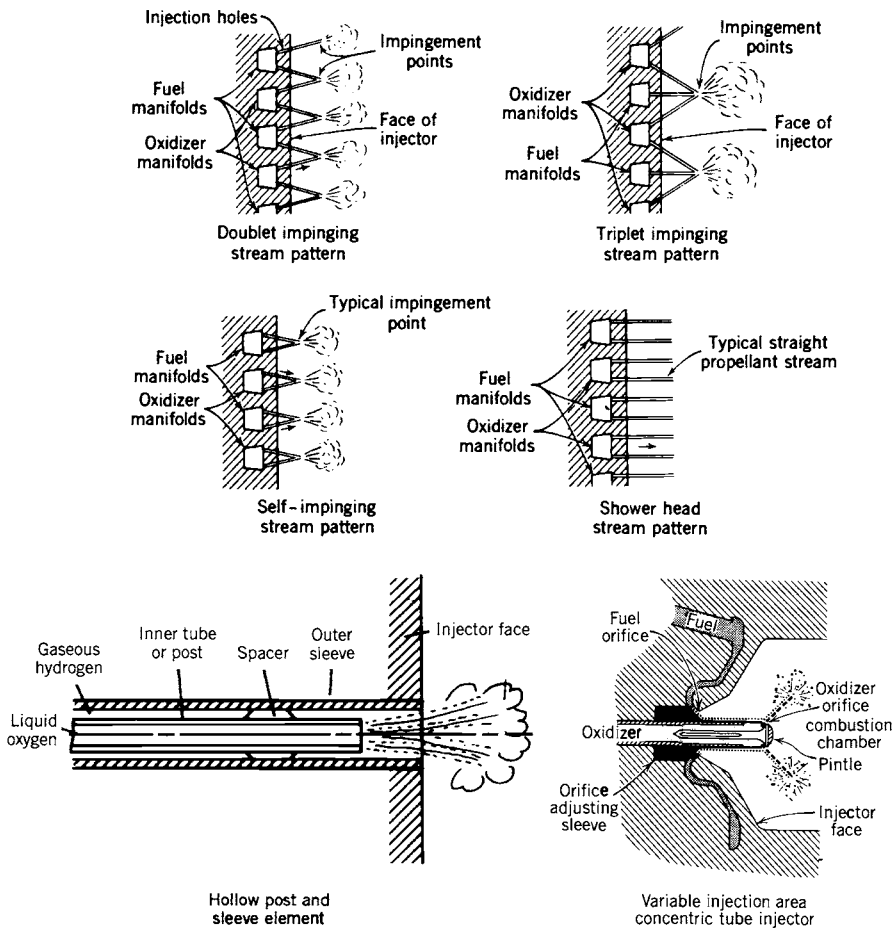


**FIGURE 8-3.** Schematic diagrams of several injector types. The movable sleeve type variable thrust injector is adapted from Ref. 8-1.

lant flow over a wide range without excessive reduction in injector pressure drop. This type of variable area concentric tube injector was used on the descent engine of the Lunar Excursion Module and throttled over a 10:1 range of flow with only a very small change in mixture ratio.

The *coaxial hollow post injector* has been used for liquid oxygen and gaseous hydrogen injectors by most domestic and foreign rocket designers. It is shown in the lower left of Fig. 8-3. It works well when the liquid hydrogen has absorbed heat from cooling jackets and has been gasified. This gasified hydrogen flows at high speed (typically 330 m/sec or 1000 ft/sec); the liquid oxygen flows far more slowly (usually at less than 33 m/sec or 100 ft/sec) and the differential velocity causes a shear action, which helps to break up the oxygen stream into small droplets. The injector has a multiplicity of these coaxial posts on its face. This

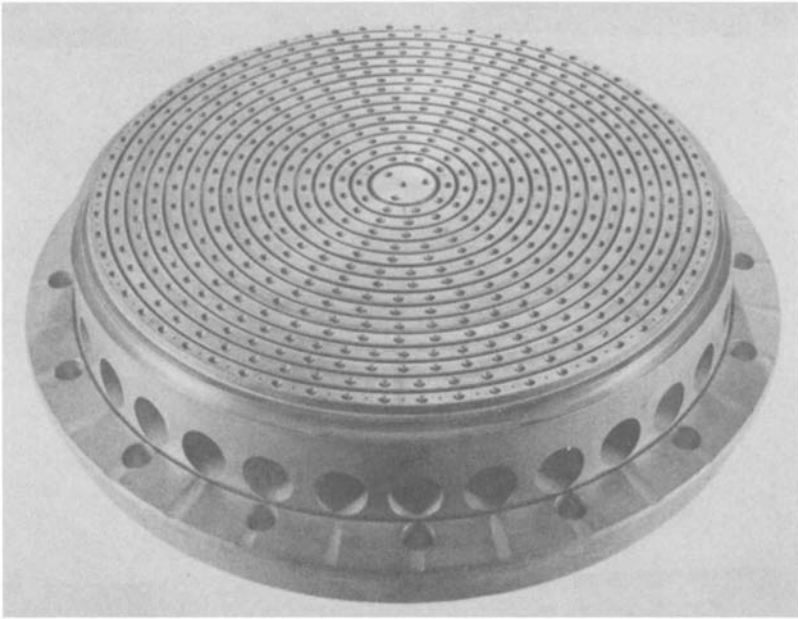


**FIGURE 8-4.** Injector with  $90^\circ$  self-impinging (fuel-against-fuel and oxidizer-against-oxidizer)-type countersunk doublet injection pattern. Large holes are inlets to fuel manifolds. Pre-drilled rings are brazed alternately over an annular fuel manifold or groove and a similar adjacent oxidizer manifold or groove. A section through a similar but larger injector is shown in Fig. 8-1.

type of injector is not used with liquid storable bipropellants, in part because the pressure drop to achieve high velocity would become too high.

The SSME injector shown in Fig. 9-6 uses 600 of these concentric sleeve injection elements; 75 of them have been lengthened beyond the injector face to form cooled baffles, which reduce the incidence of combustion instability.

The original method of making injection holes was to carefully drill them and round out or chamfer their inlets. This is still being done today. It is difficult to align these holes accurately (for good impingement) and to avoid burrs and surface irregularities. One method that avoids these problems and allows a large number of small accurate injection orifices is to use multiple etched, very thin plates (often called platelets) that are then stacked and diffusion bonded together to form a monolithic structure as shown in Fig. 8-5. The photo-etched pattern on each of the individual plates or metal sheets then provides not only for many small injection orifices at the injector face, but also for internal distribution or flow passages in the injector and sometimes also for a fine-mesh filter inside the injector body. The platelets can be stacked parallel to or normal to the injector face. The finished injector has been called the platelet injector and has been patented by the Aerojet Propulsion Company.



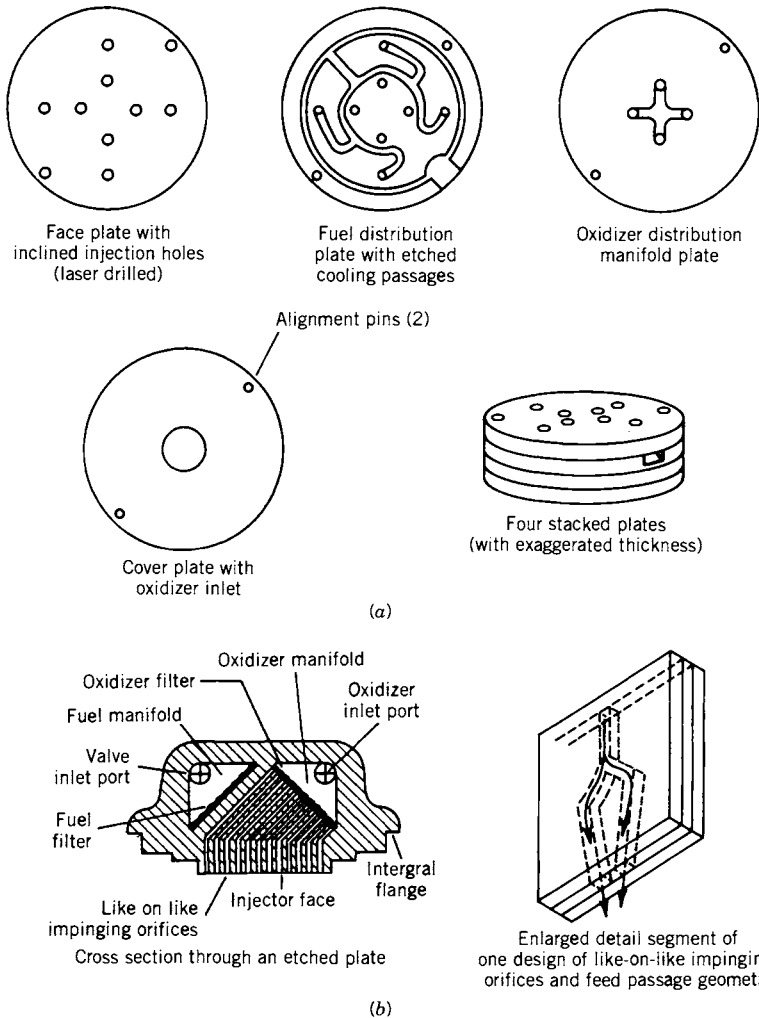


**FIGURE 8-5.** Simplified diagrams of two types of injector using a bonded platelet construction technique: (a) injector for low thrust with four impinging unlike doublet liquid streams; the individual plates are parallel to the injector face; (b) Like-on-like impinging stream injector with 144 orifices; plates are perpendicular to the injector face. (Courtesy of Aerojet Propulsion Company.)

## Injector Flow Characteristics

The differences of the various injector configurations shown in Fig. 8-3 reflect themselves in different hydraulic flow-pressure relationships, different starting characteristics, atomization, resistance to self-induced vibrations, and combustion efficiency.

The *hydraulic injector characteristics* can be evaluated accurately and can be designed for orifices with the desired injection pressures, injection velocities, flows, and mixture ratio. For a given thrust  $F$  and a given effective exhaust velocity  $c$ , the total propellant mass flow  $\dot{m}$  is given by  $\dot{m} = F/c$  from Eq. 2-6. The relations between the mixture ratio, the oxidizer, and the fuel flow rates are given by Eqs. 6-1 to 6-4. For the *flow* of an incompressible fluid through hydraulic orifices,

$$Q = C_d A \sqrt{2\Delta p / \rho} \quad (8-1)$$

$$\dot{m} = Q\rho = C_d A \sqrt{2\rho\Delta p} \quad (8-2)$$

where  $Q$  is the volume flow rate,  $C_d$  the dimensionless discharge coefficient,  $\rho$  the propellant mass density,  $A$  the cross-sectional area of the orifice, and  $\Delta p$  the pressure drop. These relationships are general and can be applied to any one section of the propellant feed system, to the injector, or to the overall liquid flow system. A typical variation of injection orifice flow and pressure drop is shown in Fig. 8-6. If the hole has a rounded entrance (top left sketch), it gives the lowest pressure drop or the highest flow. Small differences in chamfers, hole entry radius, or burrs at the edge of a hole can cause significant variations in the discharge coefficient and the jet flow patterns, and these in turn can alter

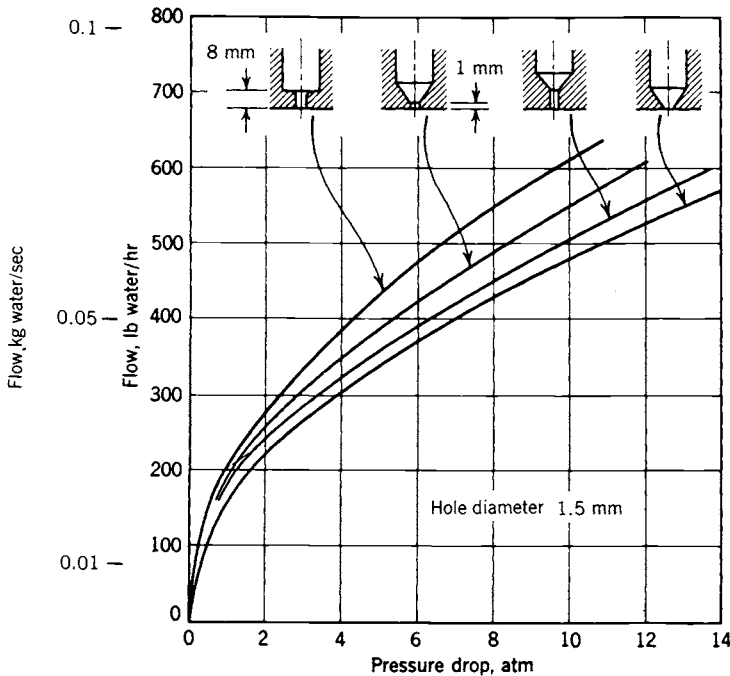


FIGURE 8-6. Hydraulic characteristics of four types of injection orifice.

the quality and distribution of the atomized small droplets, the local mixture ratio, and the local heat transfer rates. An improperly manufactured hole can cause local chamber or injector burnout.

For any given pressure drops the injection orifices determine the *mixture ratio* and the *propellant flows* of the rocket unit. From Eqs. 6-1 and 8-2 the mixture ratio is

$$r = \dot{m}_o / \dot{m}_f = [(C_d)_o / (C_d)_f] (A_o / A_f) \sqrt{(\rho_o / \rho_f) (\Delta p_o / \Delta p_f)} \quad (8-3)$$

The quantities in the preceding equations have to be chosen so that the correct design mixture ratio is attained, even if the total flow is varied slightly. Orifices whose discharge coefficients are constant over a large range of Reynolds numbers and whose ratio  $(C_d)_o / (C_d)_f$  remains invariant should be selected. For a given injector it is usually difficult to maintain the mixture ratio constant at low flows or thrusts, such as in starting.

The quality of the injector is checked by performing cold tests with inert simulant liquids instead of reactive propellant liquids. Often water is used to confirm pressure drops through the fuel or oxidizer side at different flows and this allows determination of the pressure drops with propellants and the discharge coefficients. Nonmixable inert liquids are used with a special apparatus to determine the local cold flow mixture ratio distribution over the chamber cross section. The simulant liquid should be of approximately the same density and viscosity as the actual propellant. All new injectors are hot fired and tested with actual propellants.

The actual mixture ratio can be estimated from cold flow test data, the measured hole areas, and discharge coefficients by correcting by the square root of the density ratio of the simulant liquid and the propellant. When water at the same pressure is fed alternately into both the fuel and the oxidizer sides,  $\Delta p_f = \Delta p_o$  and  $\rho_f = \rho_o$  and the water mixture ratio will be

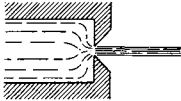
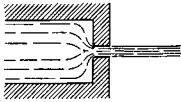
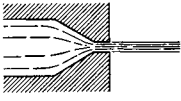
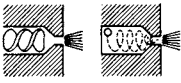
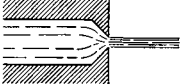
$$r = [(C_d)_o / (C_d)_f] A_o / A_f \quad (8-4)$$

Therefore, the mixture ratio measured in water tests can be converted into the actual propellant mixture ratio by multiplying it by the square root of the density ratio of the propellant combination and the square root of the pressure drop ratio. The mechanism of propellant atomization with simultaneous vaporization, partial combustion, and mixing is difficult to analyze, and performance of injectors has to be evaluated by experiment within a burning rocket thrust chamber. The *injection velocity* is given by

$$v = Q / A = C_d \sqrt{2 \Delta p / \rho} \quad (8-5)$$

Values of discharge coefficients for various types of injection orifices are shown in Table 8-2. The velocity is a maximum for a given injection pressure drop

TABLE 8-2. Injector Discharge Coefficients

Orifice Type	Diagram	Diameter (mm)	Discharge Coefficient
Sharp-edged orifice		Above 2.5 Below 2.5	0.61 0.65 approx.
Short-tube with rounded entrance $L/D > 3.0$		1.00 1.57 1.00 (with $L/D \sim 1.0$ )	0.88 0.90 0.70
Short tube with conical entrance		0.50 1.00 1.57 2.54 3.18	0.7 0.82 0.76 0.84-0.80 0.84-0.78
Short tube with spiral effect		1.0-6.4	0.2-0.55
Sharp-edged cone		1.00 1.57	0.70-0.69 0.72

when the discharge coefficient equals 1. Smooth and well-rounded entrances to the injection holes and clean bores give high values of the discharge coefficient and this hole entry design is the most common.

When an oxidizer and a fuel jet impinge, the *resultant momentum* can be calculated from the following relation, based on the principle of conservation of momentum. Figure 8-7 illustrates a pair of impinging jets and defines  $\gamma_o$  as the angle between the chamber axis and the oxidizer stream,  $\gamma_f$  as the angle between the chamber axis and the fuel stream, and  $\delta$  as the angle between the chamber axis and the average resultant stream. If the total momentum of the two jets before and after impingement is equal,

$$\tan \delta = \frac{\dot{m}_o v_o \sin \gamma_o - \dot{m}_f v_f \sin \gamma_f}{\dot{m}_o v_o \cos \gamma_o + \dot{m}_f v_f \cos \gamma_f} \quad (8-6)$$

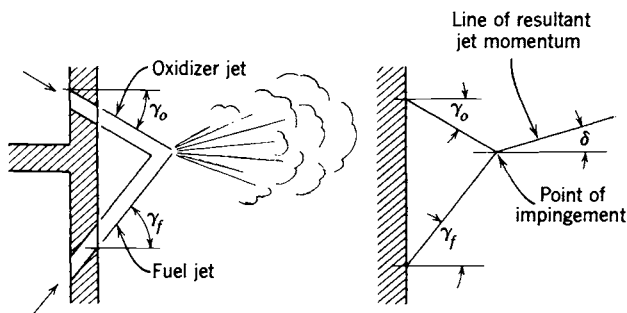


FIGURE 8-7. Angular relation of doublet impinging-stream injection pattern.

Good performance is often obtained when the resultant momentum of impinging streams is approximately axial. If the resultant momentum is along the chamber axis,  $\delta = 0$ ,  $\tan \delta = 0$ , and the angular relation for an axially directed jet momentum is given by

$$\dot{m}_o v_o \sin \gamma_o = \dot{m}_f v_f \sin \gamma_f \quad (8-7)$$

From these equations the relation between  $\gamma_f$ ,  $\gamma_o$ , and  $\delta$  can be determined. A sample injector analysis is shown in Section 8.6.

### Factors Influencing Injector Behavior

A complete theory relating injector design parameters to rocket performance and combustion phenomena has not yet been devised, and therefore the approach to the design and development of liquid propellant rocket injectors has been largely empirical. Yet the available data indicate several important factors that affect the performance and operating characteristics of injectors; some of these are briefly enumerated here.

**Propellant Combination.** The particular combination of fuel and oxidizer affects such characteristics as the relative chemical reactivity, the ease and speed of vaporization, the ignition temperature, the diffusion of hot gases, the volatility, or the surface tension. Hypergolic (self-igniting) propellants generally require injector designs somewhat different from those required by propellants that must be ignited. Injector designs that perform well with one combination generally do not work too well with a different propellant combination.

**Injection Orifice Pattern and Orifice Size.** With individual holes in the injector plate, there appears to be an optimum performance and/or heat transfer condition for each of the following parameters: orifice size, angle of impingement, angle of resultant momentum, distance of the impingement

locus from the injector face, number of injection orifices per unit of injector face surface, flow per unit of injection orifice, and distribution of orifices over the injector face. These parameters are largely determined experimentally or from similar earlier successful injectors.

**Transient Conditions.** Starting and stopping may require special provisions (temporary plugging of holes, accurate valve timing, insertion of paper cups over holes to prevent entry of one propellant into the manifold of the other propellant, or check valves) to permit satisfactory transient operation.

**Hydraulic Characteristics.** The orifice type and the pressure drop across the injection orifice determine the injection velocity. A low pressure drop is desirable to minimize the weight of the feed system or the pumping power and improve the overall rocket efficiency, yet high pressure drops are used often to increase the rocket's resistance to combustion instability and enhance atomization of the liquids.

**Heat Transfer.** Injectors influence the performance and the heat transferred in rocket thrust chambers. Low heat transfer rates have been obtained when the injection pattern resulted in an intentionally rich mixture near the chamber walls. In general, the higher performance injectors have a higher heat-transfer rate to the walls of the combustion chamber, the nozzle, and the injector face.

**Structural Design.** The injector is highly loaded by pressure forces from the combustion chamber and the propellant manifolds. During transition (starting or stopping) these pressure conditions can cause stresses which sometimes exceed the steady-state operating conditions. The faces of many modern injectors are flat and must be reinforced by suitable structures which nevertheless provide no obstructions to the hydraulic manifold passages; the structure must also be sufficiently flexible to allow thermal deformations caused by heating the injector face with hot combustion gases or cooling by cryogenic propellants. The injector design must also provide for positive seals between fuel and oxidizer manifolds (an internal leak can cause manifold explosions or internal fires) and a sealed attachment of the injector to the chamber. In large, gimbal-mounted thrust chambers the injector also often carries the main thrust load, and a gimbal mount is often directly attached to the injector, as shown in Figs. 6-1 and 8-1.

**Combustion Stability.** The injection hole pattern, impingement pattern, hole distribution, and pressure drop have a strong influence on combustion stability; some types are much more resistant to pressure disturbances. As explained in Section 9-3, the resistance to vibration is determined

experimentally, and often special antivibration devices, such as baffles or resonance cavities, are designed directly into the injector.

## 8.2. COMBUSTION CHAMBER AND NOZZLE

The *combustion chamber* is that part of a thrust chamber where the combustion or burning of the propellant takes place. The combustion temperature is much higher than the melting points of most chamber wall materials. Therefore it is necessary either to cool these walls (as described in a later section of this chapter) or to stop rocket operation before the critical wall areas become too hot. If the heat transfer is too high and thus the wall temperatures become locally too high, the thrust chamber will fail. Heat transfer to thrust chambers will be described later in this chapter. Section 8.6 gives a sample analysis of a thrust chamber and Ref. 8-2 describes the design and development of one.

### Volume and Shape

Spherical chambers give the least internal surface area and mass per unit chamber volume; they are expensive to build and several have been tried. Today we prefer a cylindrical chamber (or slightly tapered cone frustum) with a flat injector and a converging-diverging nozzle. The chamber volume is defined as the volume up to the nozzle throat section and it includes the cylindrical chamber and the converging cone frustum of the nozzle. Neglecting the effect of the corner radii, the chamber volume  $V_c$  is

$$V_c = A_1 L_1 + A_1 L_c (1 + \sqrt{A_t/A_1} + A_t/A_1) \quad (8-8)$$

Here  $L$  is the cylinder length,  $A_1/A_t$  is the chamber contraction ratio, and  $L_c$  is the length of the conical frustum. The approximate surfaces exposed to heat transfer from hot gas comprise the injector face, the inner surface of the cylinder chamber, and the inner surface of the converging cone frustum. The *volume and shape* are selected after evaluating these parameters:

1. The volume has to be large enough for adequate *mixing, evaporation, and complete combustion* of propellants. Chamber volumes vary for different propellants with the time delay necessary to vaporize and activate the propellants and with the speed of reaction of the propellant combination. When the chamber volume is too small, combustion is incomplete and the performance is poor. With higher chamber pressures or with highly reactive propellants, and with injectors that give improved mixing, a smaller chamber volume is usually permissible.
2. The chamber diameter and volume can influence the *cooling requirements*. If the chamber volume and the chamber diameter are large, the

heat transfer rates to the walls will be reduced, the area exposed to heat will be large, and the walls are somewhat thicker. Conversely, if the volume and cross section are small, the inner wall surface area and the inert mass will be smaller, but the chamber gas velocities and the heat transfer rates will be increased. There is an optimum chamber volume and diameter where the total heat absorbed by the walls will be a minimum. This is important when the available cooling capacity of the coolant is limited (for example oxygen–hydrocarbon at high mixture ratios) or if the maximum permissive coolant temperature has to be limited (for safety reasons with hydrazine cooling). The total heat transfer can also be further reduced by going to a rich mixture ratio or by adding film cooling (discussed below).

3. All inert components should have *minimum mass*. The thrust chamber mass is a function of the chamber dimensions, chamber pressure, and nozzle area ratio, and the method of cooling.
4. Manufacturing considerations favor a simple chamber geometry, such as a cylinder with a double cone bow-tie-shaped nozzle, low cost materials, and simple fabrication processes.
5. In some applications the *length* of the chamber and the nozzle relate directly to the overall length of the vehicle. A large-diameter but short chamber can allow a somewhat shorter vehicle with a lower structural inert vehicle mass.
6. The *gas pressure drop* for accelerating the combustion products within the chamber should be a minimum; any pressure reduction at the nozzle inlet reduces the exhaust velocity and the performance of the vehicle. These losses become appreciable when the chamber area is less than three times the throat area.
7. For the same thrust the combustion volume and the nozzle throat area become smaller as the operating chamber pressure is increased. This means that the chamber length and the nozzle length (for the same area ratio) also decrease with increasing chamber pressure. The performance also goes up with chamber pressure.

The preceding chamber considerations conflict with each other. It is, for instance, impossible to have a large chamber that gives complete combustion but has a low mass. Depending on the application, a compromise solution that will satisfy the majority of these considerations is therefore usually selected and verified by experiment.

The *characteristic chamber length* is defined as the length that a chamber of the same volume would have if it were a straight tube and had no converging nozzle section.

$$L^* = V_c/A_t \quad (8-9)$$



where  $L^*$  (pronounced el star) is the characteristic chamber length,  $A_t$  is the nozzle throat area, and  $V_c$  is the chamber volume. The chamber includes all the volume up to the throat area. Typical values for  $L^*$  are between 0.8 and 3.0 meters (2.6 to 10 ft) for several bipropellants and higher for some monopropellants. Because this parameter does not consider any variables except the throat area, it is useful only for a particular propellant combination and a narrow range of mixture ratio and chamber pressure. The parameter  $L^*$  was used about 40 years ago, but today the chamber volume and shape are chosen by using data from successful thrust chambers of prior similar designs and identical propellants.

The *stay time*  $t_s$  of the propellant gases is the average value of the time spent by each molecule or atom within the chamber volume. It is defined by

$$t_s = V_c / (\dot{m} \mathcal{V}_1) \quad (8-10)$$

where  $\dot{m}$  is the propellant mass flow,  $\mathcal{V}_1$  is the average specific volume or volume per unit mass of propellant gases in the chamber, and  $V_c$  is the chamber volume. The minimum stay time at which a good performance is attained defines the chamber volume that gives essentially complete combustion. The stay time varies for different propellants and has to be experimentally determined. It includes the time necessary for vaporization, activation, and complete burning of the propellant. Stay times have values of 0.001 to 0.040 sec for different types of thrust chambers and propellants.

The *nozzle* dimensions and configuration can be determined from the analyses presented in Chapter 3. The converging section of the supersonic nozzle experiences a much higher internal gas pressure than the diverging section and therefore the design of the converging wall is similar to the design of the cylindrical chamber wall. Most thrust chambers use a shortened bell shape for the diverging nozzle section. Nozzles with area ratios up to 400 have been developed.

In Chapter 3 it was stated that very large nozzle exit area ratios allow a small but significant improvement in specific impulse, particularly at very high altitudes; however, the extra length and extra vehicle mass necessary to house a large nozzle make this unattractive. This disadvantage can be mitigated by a multipiece nozzle, that is stored in annular pieces around the engine during the ascent of the launch vehicle and automatically assembled in space after launch vehicle separation and before firing. This concept, known as extendible nozzle cone, has been successfully employed in solid propellant rocket motors for space applications for about 20 years. The first flight with an extendible nozzle on a liquid propellant engine was performed in 1998 with a modified version of a Pratt & Whitney upper stage engine. Its flight performance is listed in Table 8-1. The engine is shown later in Fig. 8-19 and its carbon-carbon extendible nozzle cone is described in the section on Materials and Fabrication.

## Heat Transfer Distribution

Heat is transmitted to all internal hardware surfaces exposed to hot gases, namely the injector face, the chamber and nozzle walls. The *heat transfer rate* or *heat transfer intensity*, that is, local wall temperatures and heat transfer per unit wall area, varies within the rocket. A typical heat transfer rate distribution is shown in Fig. 8-8. Only  $\frac{1}{2}$  to 5% of the total energy generated in the gas is transferred as heat to the chamber walls. For a typical rocket of 44,820 N or 10,000 lbf thrust the heat rejection rate to the wall may be between 0.75 and 3.5 MW, depending on the exact conditions and design. See Section 8.3.

The amount of heat transferred by *conduction* from the chamber gas to the walls in a rocket thrust chamber is negligible. By far the largest part of the heat is transferred by means of *convection*. A part (usually 5 to 35%) of the transferred heat is attributable to *radiation*.

For constant chamber pressure, the chamber wall surface increases less rapidly than the volume as the thrust level is raised. Thus the cooling of chambers is generally easier in large thrust sizes, and the capacity of the wall material or the coolant to absorb all the heat rejected by the hot gas is generally more critical in smaller sizes, because of the volume-surface relationship.

Higher chamber pressure leads to higher vehicle performance (higher  $I_s$ ), but also to higher engine inert mass. However, the resulting *increase of heat transfer with chamber pressure* often imposes design or material limits on the maximum practical chamber pressure for both liquid and solid propellant rockets.

The heat transfer intensity in chemical rocket propulsion can vary from less than 50 W/cm<sup>2</sup> or 0.3 Btu/in.<sup>2</sup>-sec to over 16 kW/cm<sup>2</sup> or 100 Btu/in.<sup>2</sup>-sec. The

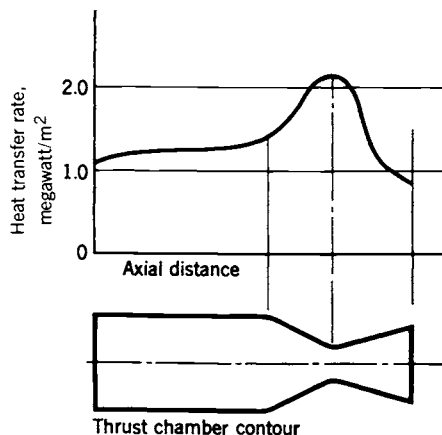


**FIGURE 8-8.** Typical axial heat transfer rate distribution for liquid propellant thrust chambers and solid propellant rocket motors. The peak is always at the nozzle throat and the lowest value is usually near the nozzle exit.

high values are for the nozzle throat region of large bipropellant thrust chambers and high-pressure solid rocket motors. The lower values are for gas generators, nozzle exit sections, or small thrust chambers at low chamber pressures.

## Cooling of Thrust Chambers

The primary objective of cooling is to prevent the chamber and nozzle walls from becoming too hot, so they will no longer be able to withstand the imposed loads or stresses, thus causing the chamber or nozzle to fail. Most wall materials lose strength and become weaker as temperature is increased. These loads and stresses are discussed in the next section. With further heating, the walls would ultimately fail or even melt. Cooling thus reduces the wall temperatures to an acceptable value.

Basically, there are two cooling methods in common use today. The first is the *steady state method*. The heat transfer rate and the temperatures of the chambers reach *thermal equilibrium*. This includes *regenerative cooling* and *radiation cooling*. The duration is limited only by the available supply of propellant.

*Regenerative cooling* is done by building a cooling jacket around the thrust chamber and circulating one of the liquid propellants (usually the fuel) through it before it is fed to the injector. This cooling technique is used primarily with bipropellant chambers of medium to large thrust. It has been effective in applications with high chamber pressure and high heat transfer rates. Also, most injectors use regenerative cooling.

In *radiation cooling* the chamber and/or nozzle have only a single wall made of high temperature material. When it reaches thermal equilibrium, this wall usually glows red or white hot and radiates heat away to the surroundings or to empty space. Radiation cooling is used with monopropellant thrust chambers, bipropellant and monopropellant gas generators, and for diverging nozzle exhaust sections beyond an area ratio of about 6 to 10 (see Fig. 8-2). A few small bipropellant thrusters are also radiation cooled. This cooling scheme has worked well with lower chamber pressures (less than 250 psi) and moderate heat transfer rates.

The second cooling method relies on *transient heat transfer* or *unsteady heat transfer*. It is also called *heat sink cooling*. The thrust chamber does not reach a thermal equilibrium, and temperatures continue to increase with operating duration. The heat absorbing capacity of the hardware determines its maximum duration. The rocket combustion operation has to be stopped just before any of the exposed walls reaches a critical temperature at which it could fail. This method has mostly been used with low chamber pressures and low heat transfer rates. Heat sink cooling of thrust chambers can be done by absorbing heat in an inner liner made of an ablative material, such as fiber-reinforced plastics. Ablative materials are used extensively in solid propellant rocket

motors and will be discussed further in Chapters 11 and 14. The analysis of both of these cooling methods is given in the next section of this chapter.

*Film cooling* and *special insulation* are supplementary techniques that are used occasionally with both methods to locally augment their cooling capability. All these cooling methods will be described further in this chapter.

Cooling also helps to reduce the oxidation of the wall material and the rate at which walls would be eaten away. The rates of chemical oxidizing reactions between the hot gas and the wall material can increase dramatically with wall temperature. This oxidation problem can be minimized not only by limiting the wall temperature, but also by burning the liquid propellants at a mixture ratio where the percentage of aggressive gases in the hot gas (such as oxygen or hydroxyl) is very small, and by coating certain wall materials with an oxidation-resistant coating; for example iridium has been coated on the inside of rhenium walls.

**Cooling with Steady-State Heat Transfer.** *Cooled thrust chambers* have provisions for cooling some or all metal parts coming into contact with hot gases, such as chamber walls, nozzle walls, and injector faces. Internal cooling passages, cooling jackets, or cooling coils permit the circulation of a *coolant*. Jackets can consist of separate inner and outer walls or of an assembly of contoured, adjacent tubes (see Figs. 8-1 and 8-9). The inner wall confines the gases, and the spaces between the walls serves as the coolant passage. The *nozzle throat region* is usually the location that has the highest heat-transfer intensity and is therefore the most difficult to cool. For this reason the cooling jacket is often designed so that the coolant velocity is highest at the critical regions by restricting the coolant passage cross section,

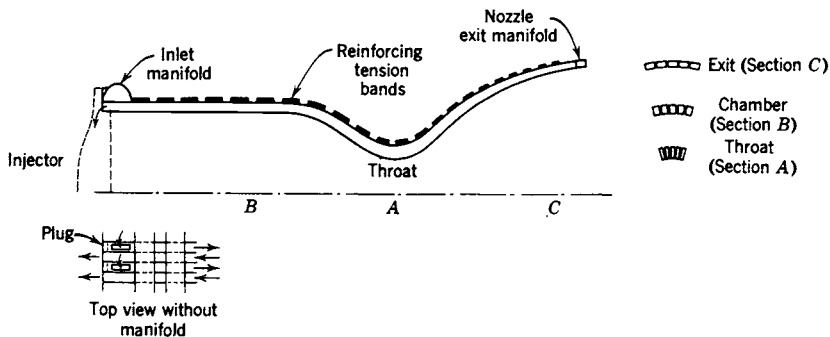


**FIGURE 8-9.** Diagram of a tubular cooling jacket. The tubes are bent to the chamber and nozzle contours; they are formed hydraulically to give a variable cross section to permit the same number of tubes at the throat and exit diameters. Coolant enters through the inlet manifold into every other tube and proceeds axially to the nozzle exit manifold, where it then enters the alternate tubes and returns axially to go directly to the injector.

and so that the fresh cold coolant enters the jacket at or near the nozzle. While the selection of the coolant velocity and its variation along the wall for any given thrust chamber design depends on heat-transfer considerations, the selection of the coolant passage geometry often depends on pressure loss, stresses, and manufacturing considerations. An *axial flow cooling jacket*, or a *tubular wall*, has a low hydraulic friction loss but is practical only for large coolant flows (above approximately 9 kg/sec). For small coolant flows and small thrust units, the design tolerances of the cooling jacket width between the inner and outer walls or the diameters of the tubes, become too small, or the tolerances become prohibitive. Therefore, most small thrust chambers use radiation cooling or ablative materials.

In *regenerative cooling* the heat absorbed by the coolant is not wasted; it augments the initial energy content of the propellant prior to injection, increasing the exhaust velocity slightly (0.1 to 1.5%). This method is called regenerative cooling because of the similarity to steam regenerators. The design of the tubular chamber and nozzle combines the advantages of a thin wall (good for reducing thermal stresses and high wall temperatures) and a cool, lightweight structure. Tubes are formed to special shapes and contours (see Figs. 8-1 and 8-9), usually by hydraulic means, and then brazed, welded, or soldered together (see Ref. 8-3). In order to take the gas pressure loads in hoop tension, they are reinforced on the outside by high-strength bands or wires. While Fig. 8-9 shows alternate tubes for up and down flow, there are chambers where the fuel inlet manifold is downstream of the nozzle throat area and where the coolant flow is up and down in the nozzle exit region, but unidirectionally up in the throat and chamber regions.

*Radiation cooling* is another steady-state method of cooling. It is simple and is used extensively in the low heat transfer applications listed previously. Further discussion of radiation cooling is given in the Materials and Fabrication subsection. In order for heat to be radiated into space, it is usually necessary for the bare nozzle and chamber to stick out of the vehicle. Figure 8-18 shows a radiation-cooled thrust chamber. Since the white hot glowing *radiation-cooled* chambers and/or nozzles are potent radiators, they may cause undesirable heating of adjacent vehicle or engine components. Therefore, many have insulation (see Fig. 8-15) or simple external radiation shields to minimize these thermal effects; however, in these cases the actual chamber or nozzle wall temperatures are higher than they would be without the insulation or shielding.

**Cooling with Transient Heat Transfer.** *Thrust chambers with unsteady heat transfer* are basically of two types. One is a *simple metal chamber* (steel, copper, stainless steel, etc.) made with walls sufficiently thick to absorb plenty of heat energy. For short-duration testing of injectors, testing of new propellants, rating combustion stability, and very-short-duration rocket-propelled missiles, such as an antitank weapon, a heavy-walled simple, short-duration steel chamber is often used. The common method of *ablative cooling* or *heat sink cooling* uses a combination of endothermic reactions

(breakdown or distillation of matrix material into smaller compounds and gases), pyrolysis of organic materials, counter-current heat flow and coolant gas mass flow, charring and localized melting. An ablative material usually consists of a series of strong, oriented fibers (such as glass, Kevlar, or carbon fibers) engulfed by a matrix of an organic material (such as plastics, epoxy resins or phenolic resins). As shown in Fig. 14-11, the gases seep out of the matrix and form a protective film cooling layer on the inner wall surfaces. The fibers and the residues of the matrix form a hard char or porous coke-like material that preserves the wall contour shapes.

The orientation, number and type of fiber determine the ability of the composite ablative material to withstand significant stresses in preferred directions. For example, internal pressure produces longitudinal as well as hoop stresses in the thrust chamber walls and thermal stresses produce compression on the inside of the walls and tensile stresses on the outside. We have learned how to place the fibers in two or three directions, which makes them anisotropic. We then speak of 2-D and 3-D fiber orientation.

A set of strong carbon fibers in a matrix of amorphous carbon is a special, but favorite type of material. It is often abbreviated as C-C or carbon-carbon. The carbon materials lose their ability to carry loads at about 3700 K or 6200 F. Because carbon oxidizes readily to form CO or CO<sub>2</sub>, its best applications are with fuel-rich propellant mixtures that have little or no free oxygen or hydroxyl in their exhaust. It is used for nozzle throat inserts. Properties for one type of C-C are given in Table 14-5.

Ablative cooling was first used and is still used extensively with solid propellant rocket motors. It has since been successfully applied to liquid propellant thrust chambers, particularly at low chamber pressure, short duration (including several short-duration firings over a long total time period) and also in nozzle extensions for both large and small thrust chambers, where the static gas temperatures are relatively low. It is not usually effective for cooling if the chamber pressures are high, the exhaust gases contain oxidative species, or the firing durations are long.

*Repeatedly starting and stopping* (also known as *pulsing*) presents a more severe thermal condition for ablative materials than operating for the same cumulative firing time but without interruption. Figure 8-10 shows that for small pulsing rockets, which fire only 4 to 15% of the time, the consumption or pyrolysis of the ablative liner is a maximum. This curve varies and depends on the specific duty cycle of firings, the design, the materials, and the pauses between the firings. The *duty cycle* for a pulsing thruster was defined in Chapter 6 as the average percent of burning or operating time divided by the total elapsed time. Between pulsed firings there is a heat soak back from the hot parts of the thruster to the cooler outer parts (causing them to become softer) and also a heat loss by radiation to the surroundings. At a duty cycle below 3%, there is sufficient time between firings for cooling by radiation. At long burning times (above 50%) the ablative material's hot layers act as insulators and prevent the stress-bearing portions from becoming too hot.

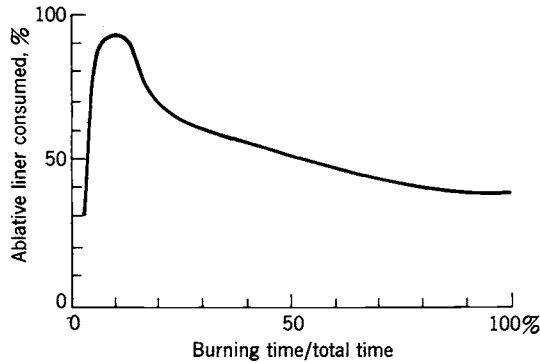


**FIGURE 8-10.** Relative depth of pyrolysis of ablative material with different duty cycles using many short-duration thrust pulses for a small liquid propellant reaction control thrust chamber of 20 lbf thrust.

Depending on the design, the thrusters with duty cycles between 4 and 25% have the most severe thermal loading.

It is often advantageous to use a different cooling method for the downstream part of the diverging nozzle section, because its heat transfer rate per unit area is usually much lower than in the chamber or the converging nozzle section, particularly with nozzles of large area ratio. There is usually a small saving in inert engine mass, a small increase in performance, and a cost saving, if the chamber and the converging nozzle section and the throat region (up to an area ratio of perhaps 5 to 10) use regenerative cooling and the remainder of the nozzle exit section is radiation cooled (or sometimes ablative cooled). See Fig. 8-2 and Ref. 8-4.

### Film Cooling

This is an auxiliary method applied to chambers and/or nozzles, augmenting either a marginal steady-state or a transient cooling method. It can be applied to a complete thrust chamber or just to the nozzle, where heat transfer is the highest. Film cooling is a method of cooling whereby a relatively cool thin fluid film covers and protects exposed wall surfaces from excessive heat transfer. Fig. 8-11 shows film-cooled chambers. The film is introduced by injecting small quantities of fuel or an inert fluid at very low velocity through a large number of orifices along the exposed surfaces in such a manner that a protective relatively cool gas film is formed. A coolant with a high heat of vaporization and a high boiling point is particularly desirable. In liquid propellant rocket engines extra fuel can also be admitted through extra injection holes at the outer layers of the injector; thus a propellant mixture is achieved (at the periphery of the chamber), which has a much lower combustion temperature. This differs from film cooling or transpiration cooling because there does not have to be a chamber

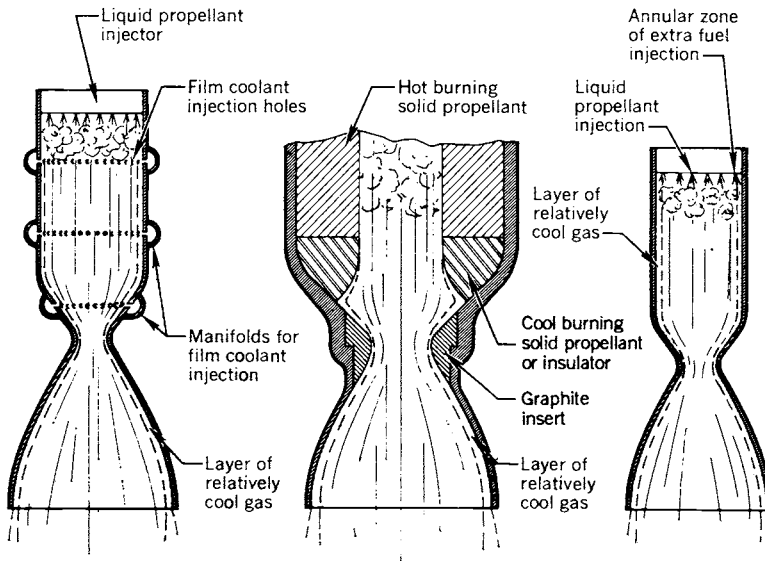


**FIGURE 8-11.** Simplified diagrams of three different methods of forming a cool boundary layer.

cooling jacket or film-cooling manifolds. In solid propellant rocket engines this can be accomplished by inserting a ring of cool-burning propellant upstream of the nozzle, as shown in Fig. 8-11 or by wall insulation materials, whose ablation and charring will release relatively cool gases into the boundary layer.

Turbine discharge gas (700 to 1100°C) has also been used as a film coolant for uncooled nozzle exit sections of large liquid propellant rocket engines. Of course, the ejection of an annular gas layer at the periphery of the nozzle exit, at a temperature lower than the maximum possible value, causes a decrease in a specific impulse. Therefore, it is desirable to reduce both the thickness of this cooler layer and the mass flow of cooler gas, relative to the total flow, to a practical minimum value.

A special type of film cooling, *sweat cooling* or *transpiration cooling*, uses a porous wall material which admits a coolant through pores uniformly over the surface. This technique has been successfully used to cool injector faces in the upper stage engine (J-2) of the moon launch vehicle and the Space Shuttle main engine (SSME) with hydrogen fuel.

### Thermal Insulation

Theoretically, a good thermal insulation layer on the gas side of the chamber wall can be very effective in reducing chamber wall heat transfer and wall temperatures. However, efforts with good insulation materials such as refractory oxides or ceramic carbides have not been successful. They will not with-



stand differential thermal expansion without cracking or spalling. A sharp edge on the surface (crack or flaked-off piece of insulator) will cause a sudden rise in the stagnation temperature and most likely lead to a local failure. Asbestos is a good insulator and was used several decades ago; because it is a cancer causing agent, it is no longer used. Coating development efforts with rhenium and other materials are continuing.

Insulation or heat shields have been successfully applied on the exterior of radiation-cooled thrust chambers to reduce the heat transfer to adjacent sensitive equipment or structures. With hydrocarbon fuels it is possible to form small carbon particles or soot in the hot gas and that can lead to a carbon deposit on the gas side of the chamber or nozzle walls. If it is a thin, mildly adhesive soot, it can be an insulator, but it is difficult to reproduce such a coating. More likely it forms hard, caked deposits, which can be spalled off in localized flakes and form sharp edges, and then it is undesirable. Most designers have preferred instead to use film cooling or extra high coolant velocities in the cooling jacket with injectors that do not create adhesive soot.

### Hydraulic Losses in the Cooling Passage

The cooling coil or cooling jacket should be designed so that the fluid adsorbs all the heat transferred across the inner motor wall, and so that the coolant pressure drop will be small.

A higher pressure drop allows a higher coolant velocity in the cooling jacket, will do a better job of cooling, but requires a heavier feed system, which increases the engine mass slightly and thus also the total inert vehicle mass. For many liquid propellant rockets the coolant velocity in the chamber is approximately 3 to 10 m/sec or 10 to 33 ft/sec and, at the nozzle throat, 6 to 24 m/sec or 20 to 80 ft/sec.

A cooling passage can be considered to be a hydraulic pipe, and the *friction loss* can be calculated accordingly. For a straight pipe,

$$\Delta p / \rho = \frac{1}{2} f v^2 (L/D) \quad (8-11)$$

where  $\Delta p$  is the friction pressure loss,  $\rho$  the coolant mass density,  $L$  the length of coolant passage,  $D$  the equivalent diameter,  $v$  the average velocity in the cooling passage, and  $f$  the friction loss coefficient. In English engineering units the right side of the equation has to be divided by  $g_0$ , the sea-level acceleration of gravity (32.2 ft/sec<sup>2</sup>). The friction loss coefficient is a function of Reynolds number and has values between 0.02 and 0.05. A *typical pressure loss* of a cooling jacket is between 5 and 25% of the chamber pressure.

A large portion of the pressure drop in a cooling jacket usually occurs in those locations where the flow direction or the flow-passage cross section is changed. Here the sudden expansion or contraction causes a loss, sometimes

larger than the velocity head  $v^2/2$ . This hydraulic situation exists in inlet and outlet chamber manifolds, injector passages, valves, and expansion joints.

The pressure loss in the cooling passages of a thrust chamber can be calculated, but more often it is measured. This pressure loss is usually determined in cold flow tests (with an inert fluid instead of the propellant and without combustion), and then the measured value is corrected for the actual propellant (different physical properties) and the hot firing conditions; a higher temperature will change propellant densities or viscosities and in some designs it changes the cross section of cooling flow passages.

### Chamber Wall Loads and Stresses

The analysis of loads and stresses is performed on all propulsion components during their engineering design. Its purpose is to assure the propulsion designer and the flight vehicle user that (1) the components are strong enough to carry all the loads, so that they can fulfill their intended function; (2) potential failures have been identified, together with the possible remedies or redesigns; and (3) their masses have been reduced to a practical minimum. In this section we concentrate on the loads and stresses in the walls of thrust chambers, where high heat fluxes and large thermal stresses complicate the stress analysis. Some of the information on safety factors and stress analysis apply also to all propulsion systems, including solid propellant motors and electric propulsion.

The safety factors (really margins for ignorance) are very small in rocket propulsion when compared to commercial machinery, where these factors can be 2 to 6 times larger. Several *load conditions* are considered for each rocket component; they are:

1. *Maximum expected working load* is the largest likely operating load under all likely operating conditions or transients. Examples are operating at a slightly higher chamber pressure than nominal as set by tolerances in design or fabrication (an example is the tolerance in setting the tank pressure regulator) or the likely transient overpressure from ignition shock.
2. *The design limit load* is typically 1.20 times the maximum expected working load, to provide a margin. If the variation in material composition, material properties, the uncertainties in the method of stress analysis, or predicted loads are significant, a larger factor may be selected.
3. *The damaging load* can be based on the yield load or the ultimate load or the endurance limit load, whichever gives the lowest value. The yield load causes a permanent set or deformation, and it is typically set as 1.10 times the design limit load. The endurance limit may be set by fatigue or creep considerations (such as in pulsing). The ultimate load induces a stress equal to the ultimate strength of the material, where significant elongation and area reduction can lead to failure. Typically it is set as 1.50 times the design limit load.

4. *The proof test load* is applied to engines or their components during development and manufacturing inspection. It is often equal to the design limit load, provided this load condition can be simulated in a laboratory. Thrust chambers and other components, whose high thermal stresses are difficult to simulate, use actual hot firing tests to obtain this proof, often with loads that approach the design limit load (for example, higher than nominal chamber pressure or a mixture ratio that results in hotter gas).

The walls of all thrust chambers are subjected to radial and axial loads from the chamber pressure, flight accelerations (axial and transverse), vibration, and thermal stresses. They also have to withstand a momentary ignition pressure surge or shock, often due to excessive propellant accumulation in the chamber. This surge can exceed the nominal chamber pressure. In addition, the chamber walls have to transmit thrust loads as well as forces and in some applications also moments, imposed by thrust vector control devices described in Chapter 16. Walls also have to survive a “thermal shock”, namely, the initial thermal stresses at rapid starting. When walls are cold or at ambient temperature, they experience higher gas heating rates than after the walls have been heated. These loads are different for almost every design, and each unit has to be considered individually in determining the wall strengths.

A heat transfer analysis is usually done only for the most critical wall regions, such as at and near the nozzle throat, at a critical location in the chamber, and sometimes at the nozzle exit. The thermal stresses induced by the temperature difference across the wall are often the most severe stresses and a change in heat transfer or wall temperature distribution will affect the stresses in the wall. Specific failure criteria (wall temperature limit, reaching yield stress, or maximum coolant temperature, etc.) have to be established for these analyses.

The temperature differential introduces a compressive stress on the inside and a tensile stress on the outside of the inner wall; the stress  $s$  can be calculated for simple cylindrical chamber walls that are thin in relation to their radius as

$$s = 2\lambda E \Delta T / (1 - \nu) \quad (8-12)$$

where  $\lambda$  is the coefficient of thermal expansion of the wall material,  $E$  the modulus of elasticity of the wall material,  $\Delta T$  the temperature drop across the wall, and  $\nu$  the Poisson ratio of the wall material. Temperature stresses frequently exceed the yield point. The materials experience a change in the yield strength and the modulus of elasticity with temperature. The preceding equation is applicable only to elastic deformations. This yielding of rocket thrust chamber wall materials can be observed by the small and gradual contraction of the throat diameter after each operation (perhaps 0.05% reduction in throat diameter after each firing) and the formation of progressive cracks of the inside

wall surface of the chamber and throat after successive runs. These phenomena limit the useful life and number of starts or temperature cycles of a thrust chamber (see Refs. 8-5 and 8-6).

In selecting a working stress for the wall material of a thrust chamber, the variation of strength with temperature and the temperature stresses over the wall thickness have to be considered. The temperature drop across the inner wall is typically between 50 and 550 K, and an average temperature is sometimes used for estimating the material properties. The most severe thermal stresses can occur during the start, when the hot gases cause thermal shock to the hardware. These transient thermal gradients cause severe thermal strain and local yielding.

A picture of a typical stress distribution caused by pressure loads and thermal gradients is shown in Fig. 8-12. Here the inner wall is subjected to a compressive pressure differential caused by a high liquid pressure in the cooling jacket and a relatively large temperature gradient. In a large rocket chamber,

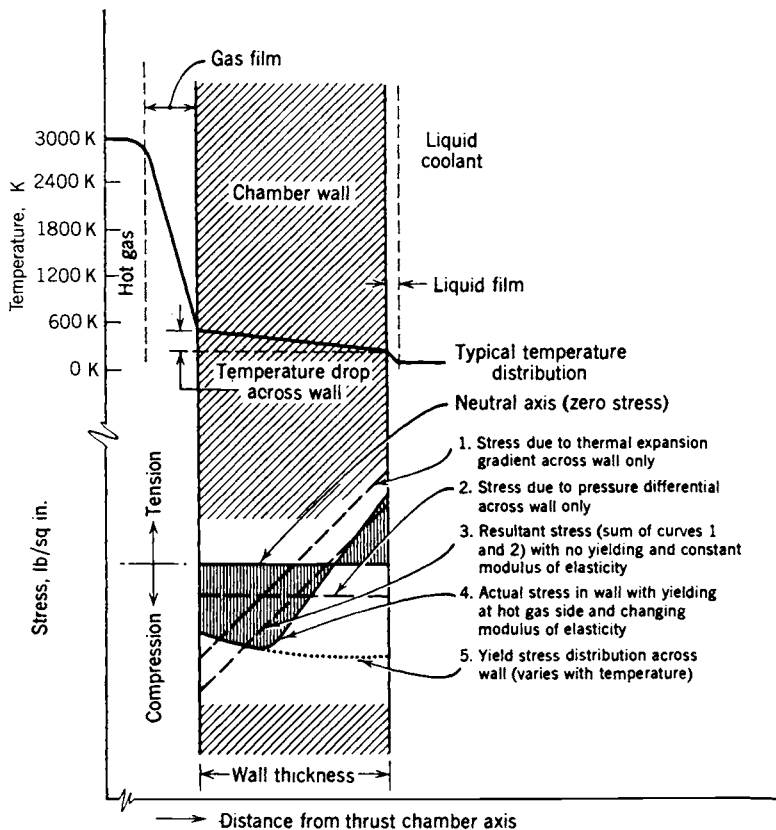


FIGURE 8-12. Typical stresses in a thrust chamber inner wall.

such as is used in the Redstone missile, the wall thickness of the nozzle steel may be 7 mm and the temperature differential across it may readily exceed several hundred degrees. This temperature gradient causes the hot inner wall surface to expand more than the wall surface on the coolant side and imposes a high compressive thermal stress on the inside surface and a high tensile thermal stress on the coolant side. In these thick walls the stress induced by the pressure load is usually small compared to the thermal stress. The resultant stress distribution in thick inner walls (shown shaded in the sample stress diagram of Fig. 8-12) indicates that the stress in the third of the wall adjacent to the hot gases has exceeded the yield point. Because the modulus of elasticity and the yield point diminish with temperature, the stress distribution is not linear over the yielded portion of the wall. In effect, this inner portion acts as a heat shield for the outer portion which carries the load.

Because of the differential expansion between the hot inner shell and the relatively cold outer shell, it is necessary to provide for axial *expansion joints* to prevent severe temperature stresses. This is particularly critical in larger double-walled thrust chambers. The German V-2 thrust chamber expanded over 5 mm in an axial and 4 mm in a radial direction.

Tubes for tubular wall thrust chambers are subjected to several different stress conditions. Only that portion of an individual cooling tube exposed to hot chamber gases experiences high thermal stresses and deformation as shown in Fig. 8-17. The tubes have to hold the internal coolant pressure, absorb the thermal stresses, and contain the gas pressure in the chamber. The hottest temperature occurs in the center of the outer surface of that portion of each tube exposed to hot gas. The thermal stresses are relatively low, since the temperature gradient is small; copper has a high conductivity and the walls are relatively thin (0.5 to 2 mm). The coolant pressure-induced load on the tubes is relatively high, particularly if the thrust chamber operates at high chamber pressure. The internal coolant pressure tends to separate the tubes. The gas pressure loads in the chamber are usually taken by reinforcing bands which are put over the outside of the tubular jacket assembly (see Fig. 8-1 and 8-9). The joints between the tubes have to be gas tight and this can be accomplished by soldering, welding, or brazing.

When a high-area-ratio nozzle is operated at high ambient pressure, the lower part of the nozzle structure experiences a compression because the pressure in the nozzle near the exit is actually below atmospheric value. Therefore, high-area-ratio nozzles usually have stiffening rings on the outside of the nozzle near the exit to maintain a circular shape and thus prevent buckling, flutter, or thrust misalignment.

### **Aerospike Thrust Chamber**

A separate category comprises thrust chambers using a center body, such as a plug nozzle or aerospike nozzle. They have more surface to cool than ordinary thrust chambers. A circular aerospike thruster is described in Chapter 3 and

shown schematically in Fig. 3–12. Here the diameter of the exhaust flow plume increases with altitude. A linear version of a truncated (shortened) aerospike thrust chamber is currently being developed with liquid oxygen and liquid hydrogen as the propellants; see Refs. 8–7 and 8–8. An experimental engine; assembly (XRS-2200) with 20 cells and two hydrogen-cooled, two-dimensional, curved ramps is shown in Figs 8–13 and 8–14. Each individual small (regeneratively cooled) thrust chamber or cell has its own cylindrical combustion chamber, a circular small nozzle throat, but a rectangular nozzle exit of low area ratio. The gas from these 20 rectangular nozzle exits is further expanded (and thus reaches a higher exhaust velocity) along the contour of the spike or ramp. The two fuel-cooled side panels are not shown in these figures. The flat surface at the bottom or base is porous or full of small holes and a low-pressure gas flows through these openings. This causes a back pressure on the flat base surface. This flow can be the exhaust gas from the turbopumps and is typically 1 or 2% of the total flow. The gas region below this base is enclosed by the two gas flows from the ramps and the two side plates and is essentially independent of ambient pressure or altitude. Two of the XRS-2200 engine drive the X-33 wing shaped vehicle aimed at investigating a single stage to orbit concept.

The thrust  $F$  of this aerospike thrust chamber consists of (1) the axial component thrusts of each of the little chamber modules, (2) the integral of the pressures acting on the ramps over the axially projected area  $A_a$  normal to the axis of the ramps, and (3) the pressure acting over the base area  $A_{\text{base}}$ .

$$F = [\dot{m}v_2 \cos \theta + (p_2 - p_3)A_2 \cos \theta] + 2 \int_{A_a} p \, dA + (p_{\text{base}} - p_3)A_{\text{base}} \quad (8-13)$$

Here  $\theta$  is the angle of the module nozzle axis to the centerline of the spike,  $\dot{m}$  is the total propellant flow,  $v_2$  is the exhaust velocity of the module,  $A_2$  is the total exit area of all the modules,  $p_2$  is the exhaust pressure at the exit of the module, and  $p_3$  is the ambient pressure at the nozzle exit level. These expressions are a simplified version of the thrust. Not included, for example, is the negative effect of the slipstream of air around the engine (which causes a low-pressure region) and the friction on the side plates; both actually decrease the thrust slightly. For each application there is an optimum angle  $\theta$ , an optimum ramp length, an optimum ratio of the projected ramp area to the base area, and an optimum base pressure, which is a function of the base flow.

The local gas pressures on the ramps are influenced by shock wave phenomena and change with altitude. Figure 8–14 shows a typical pressure distribution on a typical ramp surface and the flow patterns for low and high altitude. The hot gas flows coming out of the cell nozzles are turned into a nearly axial direction by multiple expansion waves (shown as dashed lines), which cause a reduction in pressure. At lower altitudes the turning causes compression shock waves (represented as solid lines), which causes local pressures to rise. The compression waves are reflected off the boundary between the hot gas jet

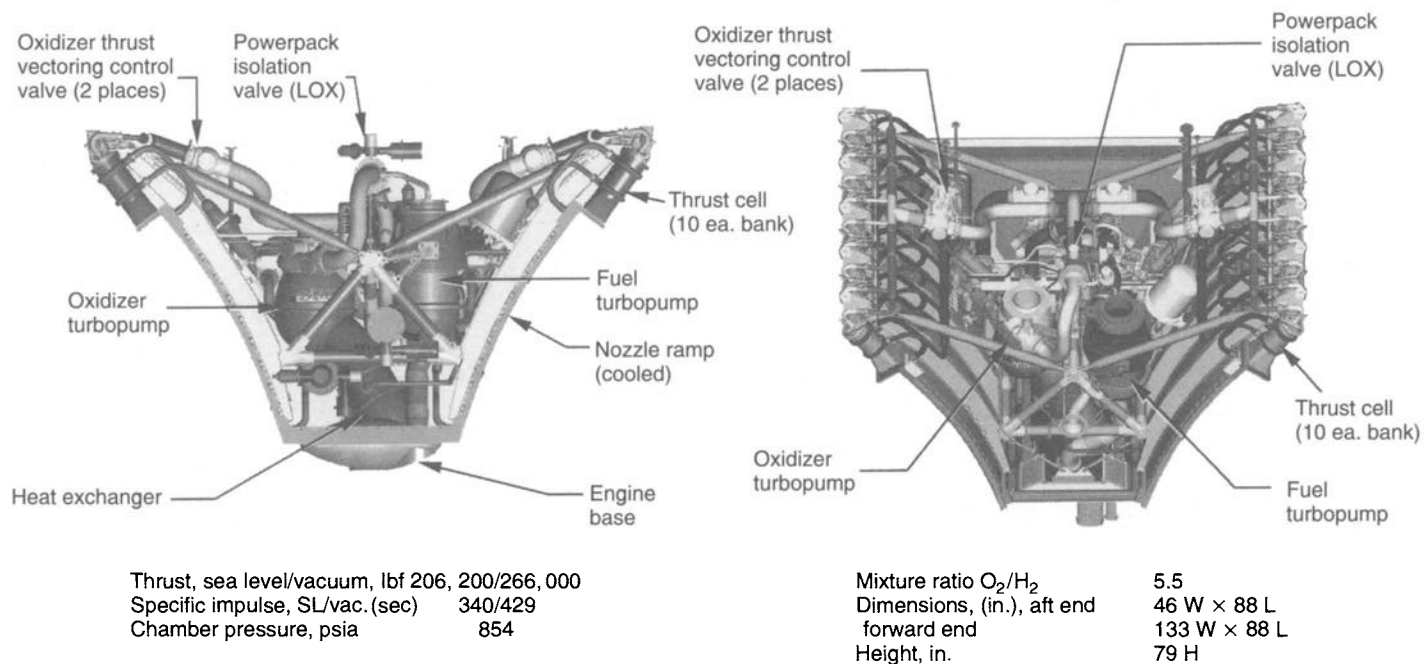


**FIGURE 8-13.** Side view and oblique top view of the XRS-2200 aerospike linear rocket engine with 20 thrust cells and two curved fuel-cooled ramps. (Courtesy of The Boeing Company, Rocketdyne Propulsion and Power.)

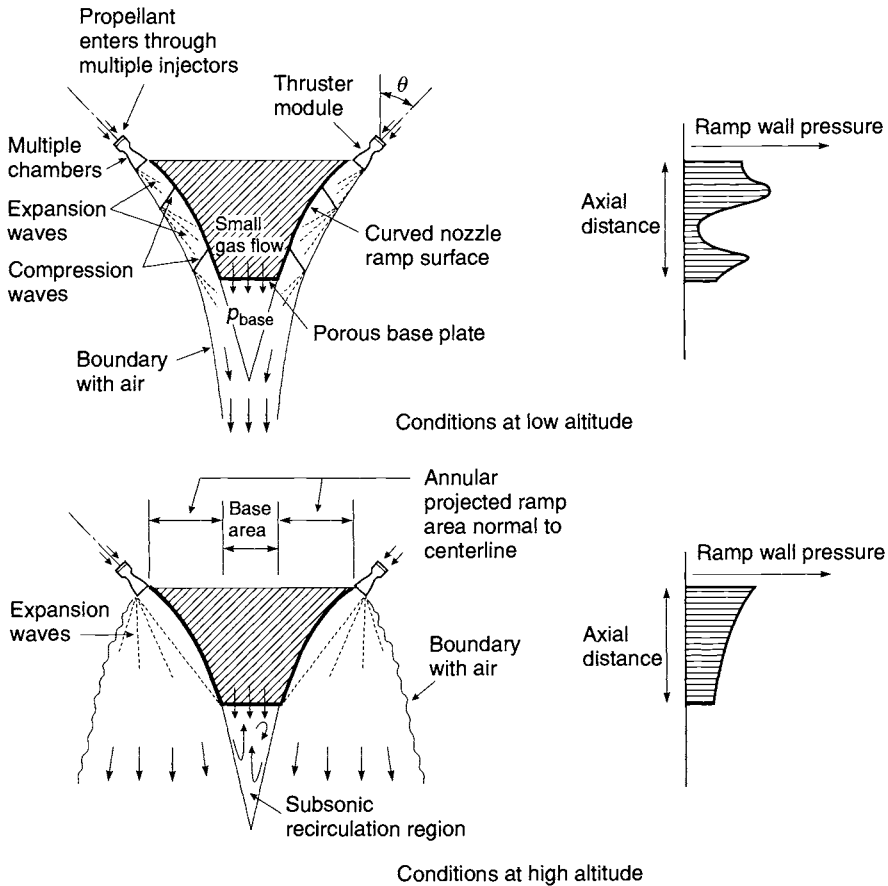


**FIGURE 8-14.** Pressure profile and flow pattern along the ramp of an aerospike nozzle.

and the ambient air stream, creating further expansion waves. At high altitude there are no compression waves emanating from the ramp and the expanding diverging flow exerts a decreasing pressure on the ramp area and behaves very similarly to the diverging nozzle flow in a bell-shaped conventional nozzle exit section. The contact locations, where the compression waves touch the ramp surface, have higher local heat transfer than other areas on the ramp surface; these locations move downstream as the vehicle gains altitude. The wave patterns and the pressure distribution on the spike or ramp surface can be determined from computerized fluid dynamics programs or a method of characteristics program.

The *advantages* claimed for a linear aerospike engine are these: (1) compared to the axisymmetric rocket engine, it fits well into the trailing edge of a winged or lifting body type vehicle and often has less engine and structural mass; (2) it has altitude compensation and thus operates at optimum nozzle expansion and



highest possible performance at every altitude; (3) differential throttling of certain sets of individual thruster modules allows pitch, yaw, and roll control of the vehicle during powered flight, as explained in Chapter 16. There is no gimbal joint, no movement of the nozzle, no actuators, and no actuator power supply or strong structural locations for actuator side loads; (4) the truncated aerospike is short and requires less vehicle volume and structures; and (5) the engine structure can be integrated with the vehicle structure, avoiding a separate vehicle structure at or near the engines. The *disadvantages* include the lack of proven flight experience, proven reliability and performance validation (which are expected to happen soon), and a larger-than-usual surface area subject to high heat transfer.

### Low-Thrust Rocket Thrust Chambers or Thrusters

Spacecraft, certain tactical missiles, missile defense vehicles, and upper stages of ballistic missiles often use special, multiple thrusters in their small, liquid propellant rocket engines. They generally have thrust levels between about 0.5 and 10,000 N or 0.1 to 2200 lbf, depending on vehicle size and mission. As mentioned in Chapter 4, they are used for trajectory corrections, attitude control, docking, terminal velocity control in spacecraft or ballistic missiles, divert or side movement, propellant settling, and other functions. Most operate with multiple restarts for relatively short durations during a major part of their duty cycle. As mentioned in Chapter 6, they can be classified into *hot gas thrusters* (high-performance bipropellant with combustion temperatures above 2600 K and  $I_s$  of 200 to 325 sec), *warm gas thrusters* such as monopropellant hydrazine (temperatures between 500 and 1600 K and  $I_s$  of 18 to 245 sec), and *cold gas thrusters* such as high-pressure stored nitrogen (200 to 320 K) with low specific impulses (40 to 120 sec).

A typical small thruster for bipropellant is shown in Fig. 8-15 and for hydrazine monopropellant in Fig. 8-16. For attitude control angular motion these thrust chambers are usually arranged in pairs as explained in Section 4.6. The same control signal activates the valves for both units of such a pair. All these small space rocket systems use a pressurized feed system, some with positive expulsion provisions, as explained in Section 6.3. The vehicle mission and the automatic control system of the vehicle often require irregular and frequent pulses to be applied by pairs of attitude control thrust chambers, which often operate for very short periods (as low as 0.01 to 0.02 sec). This type of frequent and short-duration thrust application is also known as *pulsed thrust operation*. For translation maneuvers a single thruster can be fired (often in a pulsing mode) and the thrust axis usually goes through the center of gravity of the vehicle. The resulting acceleration will depend on the thrust and the location of the thruster on the vehicle; it can be axial or at an angle to the flight velocity vector.

There is a performance degradation with decreasing pulse duration, because propellants are used inefficiently during the buildup of thrust and the decay of

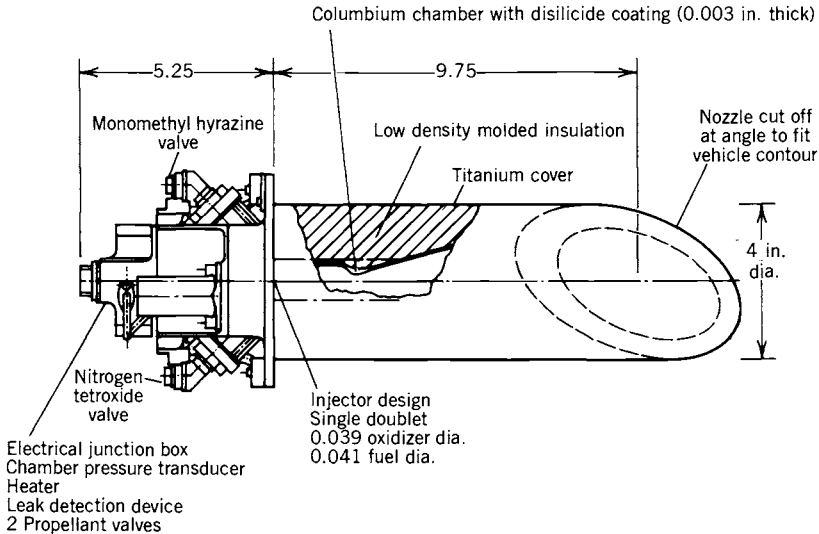


**FIGURE 8-15.** This radiation-cooled, insulated vernier thruster is one of several used on the Reaction Control System of the Space Shuttle vehicle for orbit stabilization and orientation, rendezvous or docking maneuvers, station keeping, deorbit, or entry. The nozzle is cut off at an angle to fit the contour of the vehicle. Performance data are given in Table 6-3. Operation can be in a pulse mode (firing durations between 0.08 and 0.32 sec with minimum offtime of 0.08 sec) or a steady-state mode (0.32 to 125 sec). Demonstrated life is 23 hr of operation and more than 300,000 starts. (Courtesy of Kaiser Marquardt Company and NASA.)

thrust, when they operate below full chamber pressure and the nozzle expansion characteristics are not optimum. The specific impulse suffers when the pulse duration becomes very short. In Section 3-5 the actual specific impulse of a rocket operating at a steady state was given at about 92% of theoretical specific impulse. With very short pulses (0.01 sec) this can be lower than 50%, and with pulses of 0.10 sec it can be around 75 to 88%. Also, the reproducibility of the total impulse delivered in a short pulse is not as high after prolonged use. A preheated monopropellant catalyst bed will allow performance improvement in the pressure rise and in short pulses.

One way to minimize the impulse variations in short pulses and to maximize the effective actual specific impulse is to minimize the liquid propellant passage volume between the control valve and the combustion chamber. The propellant flow control valves for pulsing attitude control thrust chambers are therefore often designed as an integral part of the thrust chamber-injector assembly, as shown in Fig. 8-15. Special electrically actuated leakproof, fast-acting valves with response times ranging from 2 to 25 msec for both the opening and closing operation are used. Valves must operate reliably with predictable characteristics for perhaps 40,000 to 80,000 starts. This in turn often requires endurance proof tests of 400,000 to 800,000 cycles.

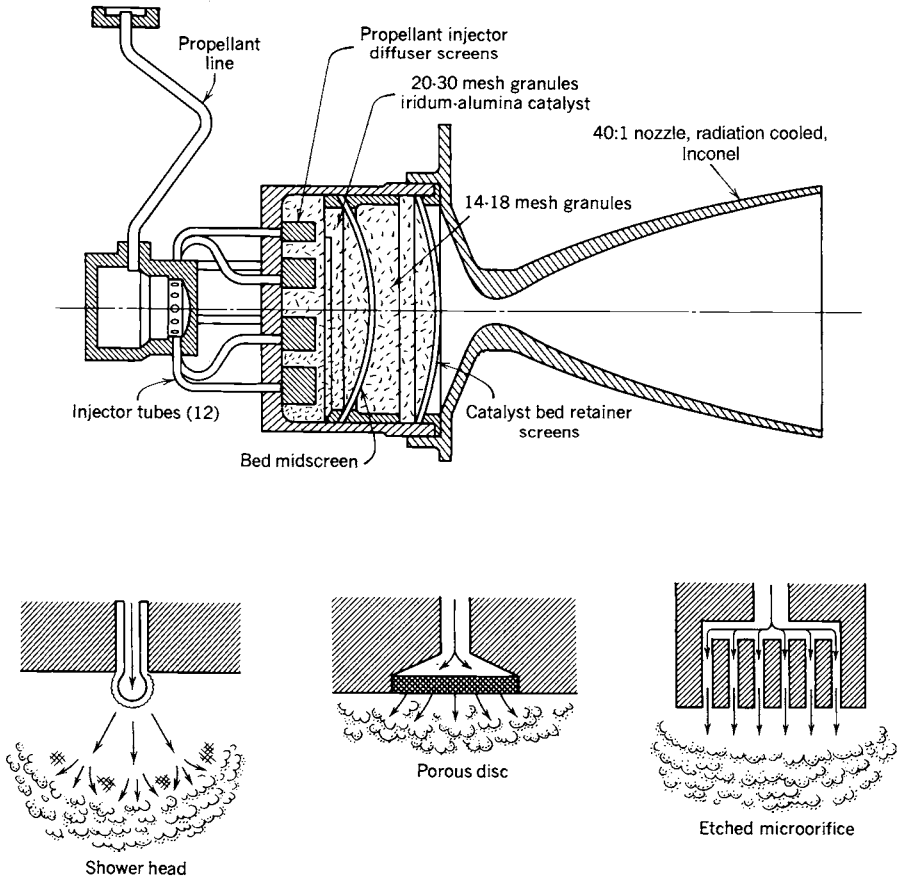


**FIGURE 8-16.** Typical hydrazine monopropellant small thrust chamber with catalyst bed, showing different methods of injection.

Liquid storable bipropellants such as  $N_2O_4$ -monomethylhydrazine are used when high performance is mandatory. Some have used ablative materials for thrust chamber construction, as in the Gemini command module. The Space Shuttle small thrusters use radiation cooling with refractory metals, as shown in Fig. 8-15. A radiation cooled thruster is shown later in Fig. 8-18. Carbon materials made of woven strong carbon fibers in a matrix of carbon have also been used in radiation-cooled bipropellant thrusters.

Hydrazine monopropellant thrusters are used when system simplicity is important and moderate performance is acceptable. They have a nontoxic, clear, clean exhaust plume. Virtually all hydrazine monopropellant attitude control rockets use finely dispersed iridium or cobalt deposited on porous ceramic (aluminum oxide) substrate pellets 1.5 to 3 mm in diameter as a catalyst. Figure 8-16 shows a typical design of the catalyst pellet bed in an

attitude control rocket designed for pulse and steady-state operation meeting a specific duty cycle. Each injection hole is covered with a cylindrical screen section which extends into a part of the catalyst bed and distributes the hydrazine propellant. Fig. 8-16 also shows other successful types of hydrazine injector. Several arrangements of catalyst beds are employed; some have spring-loading to keep the pellets firmly packed. Hydrazine monopropellant thrust units range in size from 0.2 to 2500 N of thrust; the scaling procedure is empirical and each size and design requires testing and retesting. The amount of ammonia decomposition, shown in Fig. 7-3, can be controlled by the design of the catalyst bed and its decomposition chamber.

Mechanical, thermal, and chemical problems arise in designing a catalyst bed for igniting hydrazine, the more important of which are catalytic attrition and catalyst poisoning. *Catalytic attrition* or physical loss of catalyst material stems from motion and abrasion of the pellets, with loss of very fine particles. Crushing of pellets can occur because of thermal expansion and momentary overpressure spikes. As explained in Chapter 7, the catalyst activity can also decline because of *poisoning* by trace quantities of contaminants present in commercial hydrazine, such as aniline, monomethylhydrazine, unsymmetrical dimethylhydrazine, sulfur, zinc, sodium, or iron. Some of these contaminants come with the hydrazine and some are added by the tankage, pressurization, and propellant plumbing in the spacecraft. The high-purity grade has less than 0.003% aniline and less than 0.005% carbonaceous material; it does not contaminate catalysts. Catalyst degradation, regardless of cause, produces ignition delays, overpressures, and pressure spikes, decreases the specific impulse, and decreases the impulse duplicate bit per pulse in attitude control engines.

Figure 19-4 shows a combination of chemical monopropellant and electrical propulsion. Electrical post-heating of the reaction gases from catalysis allows an increase of the altitude specific impulse from 240 sec to about 290 or 300 sec. A number of these combination auxiliary thrusters have successfully flown on a variety of satellite applications and are particularly suitable for spacecraft where electrical power is available and extensive short-duration pulsing is needed.

*Cold gas thrusters* and their performance were mentioned in Section 6.8 and their propellants and specific impulses are listed in Table 7-3. They are simple, low cost, used with pressurized feed systems, used for pulsing operations, and for low thrust and low total impulse. They can use aluminum or plastics for thrusters, valves and piping. The Pegasus air-launched launch vehicle uses them for roll control only. The advantages of cold gas systems are: (a) they are very reliable and have been proven in space flights lasting more than 10 years; (b) the system is simple and relatively inexpensive; (c) the ingredients are nontoxic; (d) no deposit or contamination on sensitive spacecraft surfaces, such as mirrors; (e) they are very safe; and (f) capable of random pulsing. The disadvantages are: (a) engines are relatively heavy with poor propellant mass fractions (0.02 to 0.19); (b) the specific impulses and vehicle velocity increments

are low, when compared to mono- or bipropellant systems; and (c) relatively large volumes.

## Materials and Fabrication

The choice of the material for the inner chamber wall in the chamber and the throat region, which are the critical locations, is influenced by the hot gases resulting from the propellant combination, the maximum wall temperature, the heat transfer, and the duty cycle. Table 8-3 lists typical materials for several thrust sizes and propellants. For high-performance, high heat transfer, regeneratively cooled thrust chambers a material with high thermal conductivity and a thin wall design will reduce the thermal stresses. Copper is an excellent conductor and it will not really oxidize in fuel-rich non-corrosive gas mixtures, such as are produced by oxygen and hydrogen below a mixture ratio of 6.0. The inner walls are therefore usually made of a copper alloy (with small additions of zirconium, silver, or silicon), which has a conductivity not quite as good as pure (oxygen-free) copper but has improved high temperature strength.

Figure 8-17 shows a cross section of a cooling jacket for a large, regeneratively cooled thrust chamber with formed tapered tubes that are brazed together. The other fabrication technique is to machine nearly rectangular grooves of variable width and depth into the surface of a relatively thick contoured high-conductivity chamber and nozzle wall liner; the grooves are then filled with wax and, by an electrolyte plating technique, a wall of nickel is added to enclose the coolant passages (see Fig. 8-17). The wax is then melted out. As with tubular cooling jackets, a suitable inlet and outlet manifolds are needed to distribute and collect the coolant flow. The figure also shows the locations of maximum wall temperature. For propellant combinations with corrosive or aggressive oxidizers (nitric acid or nitrogen tetroxide) stainless steel is often used as the inner wall material, because copper would chemically react. The depth and width of milled slots (or the area inside formed tubes) vary with the chamber-nozzle profile and its diameters. At the throat region the cooling velocity needs to be at its highest and therefore the cooling passage cross section will be at its lowest.

The failure modes often are bulging on the hot gas side and the opening up of cracks. During hot firing the strain at the hot surface can exceed the local yield point, thus giving it a local permanent compressive deformation. With the cooldown after operation and with each successive firing, some additional yielding and further plastic deformation will occur until cracks form. With successive firings the cracks can become deep enough for a leak and the thrust chamber will then usually fail. The *useful life* of a metal thrust chamber is the maximum number of firings (and sometimes also the cumulative firing duration) without such a failure. The prediction of wall failures is not simple and Refs. 8-5 and 8-6 explain this in more detail. Useful life can also be limited by the storage life of soft components (O-rings, gaskets, valve stem lubricant) and,

**TABLE 8-3.** Typical Materials used in Several Common Liquid Propellant Thrust Chambers

Application	Propellant	Components	Cooling Method	Typical Materials
Bipropellant TC, cooled, high pressure (Booster or upper stage)	Oxygen-hydrogen	C, N, E	F	Copper alloy
		I	F	Transpiration cooled porous stainless steel face. Structure is stainless steel
		Alternate E	R	Carbon fiber in a carbon matrix, or niobium
	Same	Alternate E	T	Steel shell with ablative inner liner
		C, N, E, I	F	Stainless steel with tubes or milled slots
Experimental TC (very limited duration—only a few seconds)	All types	C, N, E	U	Carbon fiber in a carbon matrix, or niobium
				Steel shell with ablative inner liner
				Low carbon steel
Small bipropellant TC	All types	C, N, E	R	Carbon fiber in carbon matrix, rhenium, niobium
			T	Steel shell with ablative inner liner
		I	F	Stainless steels, titanium
Small monopropellant TC	Hydrazine	C, N, E, I	R	Inconel, alloy steels
			F	Stainless steel
Cold gas TC	Compressed air, nitrogen	C, N, E, I	U	Aluminum, steel or plastic

\* $\text{HNO}_3$  or  $\text{N}_2\text{O}_4$  oxidizer with  $\text{N}_2\text{H}_4$ , MMH, or UDMH as fuels (see Chapter 7). TC = thrust chamber, C = chamber wall, N = nozzle converging section wall and throat region walls, E = walls at exit region of diverging section of nozzle, I = injector face, F = fuel cooled (regenerative), R = radiation cooled, U = uncooled, T = transient heat transfer or heat sink method (ablative material).

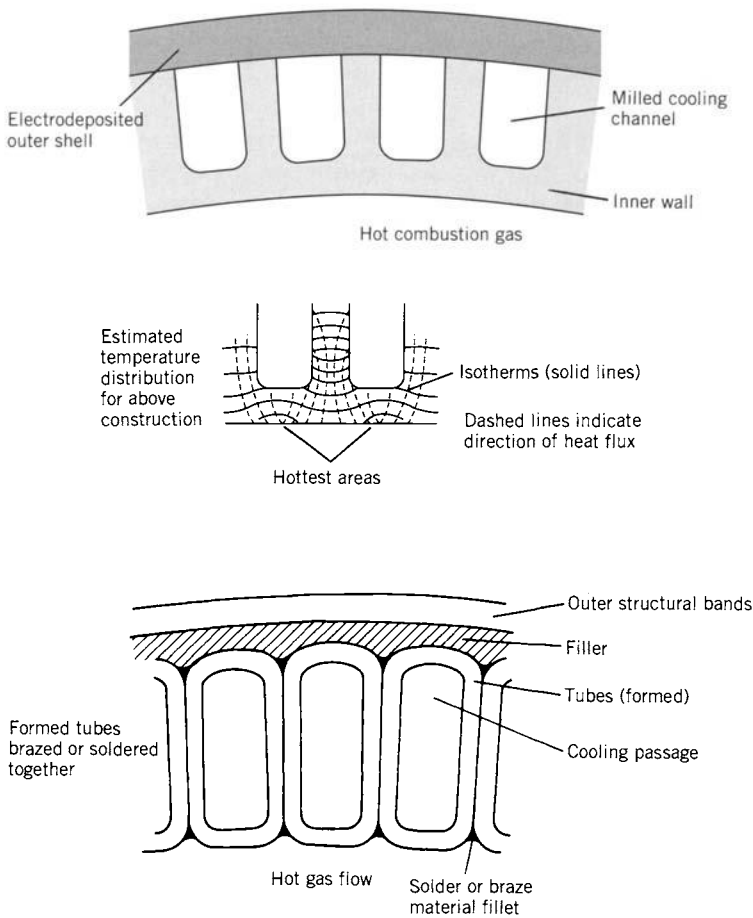


**FIGURE 8-17.** Enlarged cross section of thrust chamber's regenerative cooling passages for two types of design.

for small thrusters with many pulses, also the fatigue of valve seats. Therefore, there is a maximum limit on the number of firings that such a thrust chamber can withstand safely, and this limits its *useful life* (see Refs. 8-7 and 8-8).

For *radiation cooling*, several different carbon materials have worked in a reducing, fuel-rich rocket atmosphere. At other gas mixtures they can oxidize at the elevated temperatures when they glow red or white. They can be used at wall temperatures up to perhaps 3300 K or 6000 R. Carbon materials and ablative materials are used extensively in solid propellant rocket motors and are discussed further in Chapter 14.

For some small radiation-cooled bipropellant thrusters with storable propellants, such as those of the reaction control thrusters on the Space Shuttle Orbiter, the hot walls are made of niobium coated with disilicide (up to 1120 K

or 2050 R). To prevent damage, a fuel-rich mixtures or film cooling is often used. Rhenium walls protected by iridium coatings (oxidation resistant) have come into use more recently and can be used up to about 2300 K or 4100 R (see Ref. 8–9). Other high temperature materials, such as tungsten, molybdenum, alumina, or tantalum, have been tried, but have had problems in manufacture, cracking, hydrogen embrittlement, and excessive oxidation.

A small radiation-cooled monopropellant thruster is shown in Fig. 8–16 and a small radiation cooled bipropellant thruster in Fig. 8–18. This thruster's injection has extra fuel injection holes (not shown in Fig. 8–18) to provide film cooling to keep wall temperatures below their limits. This same thruster will also work with hydrazine as the fuel.

Until recently it has not been possible to make large pieces of carbon-carbon material. This was one of the reasons why large nozzle sections and integral nozzle-exit-cone pieces in solid motors were made from carbon phenolic cloth lay-ups. Progress in manufacturing equipment and technology has now made it possible to build and fly larger c-c pieces. A three-piece extendible c-c nozzle exit cone of 2.3 m (84 in.) diameter and 2.3 to 3 mm thickness has recently flown on an upper-stage engine. This engine with its movable nozzle

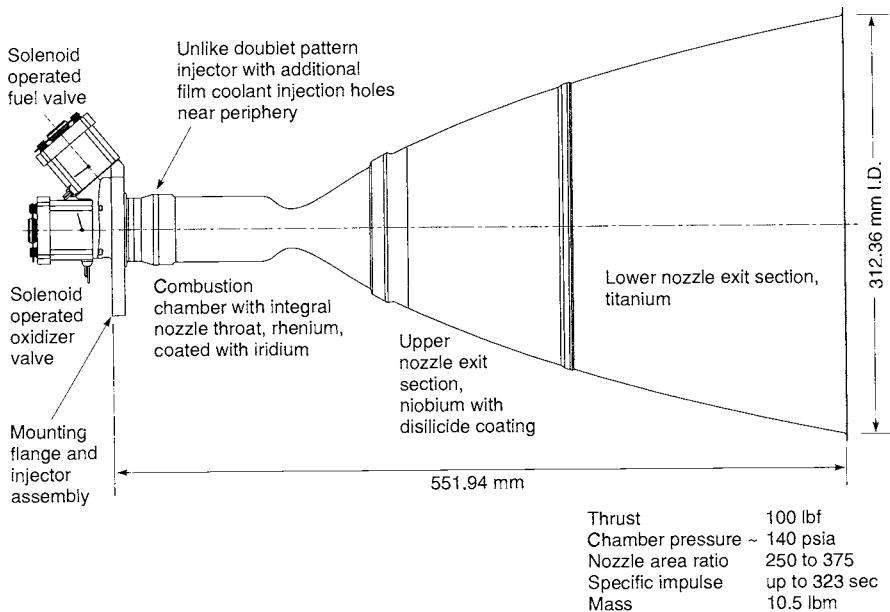


**FIGURE 8–18.** Radiation-cooled reaction control thruster R-4D-15 uses nitrogen tetroxide and monomethylhydrazine propellants. The large nozzle area ratio allows good vacuum performance. It has three different nozzle materials, each with a lower allowable temperature (Re 4000°F; Nb 3500°F; Ti 1300°F. (Courtesy of Kaiser-Marquardt Company.)



extension is shown in Fig. 8-19, its parameters are listed in Table 8-1, and its testing is reported in Ref. 8-4.

The material properties have to be evaluated before a material can be selected for a specific thrust chamber application. This evaluation includes physical properties, such as tensile and compressive strengths, yield strength, fracture toughness, modulus of elasticity (for determining deflections under load), thermal conductivity (a high value is best for steady-state heat transfer), coefficient of thermal expansion (some large thrust chambers grow by 3 to 10 mm when they become hot, and that can cause problems with their piping connections or structural supports), specific heat (capacity to absorb thermal energy), reflectivity (for radiation), or density (ablatives require more volume than steel). All these properties change with temperature (they are different when they are hot) and sometimes they change with little changes in composition. The temperature where a material loses perhaps 60 to 75% of its room temperature strength is often selected as the maximum allowable wall temperature, well below its melting point. Since a listing of all the key properties of a single material requires many pages, it is not possible to list them here, but they are usually available from manufacturers and other sources. Other important properties are erosion resistance, little or no chemical reactions with the propellants or the hot gases, reproducible decomposition or vaporization of ablative materials, ease and low cost of fabrication (welding, cutting, forming, etc.), the consistency of the composition (impurities) of different batches of each material (metals, organics, seals, insulators, lubricants, cleaning fluids), and ready availability and low cost of each material.

### 8.3. HEAT TRANSFER ANALYSIS

In actual rocket development not only is the heat transfer analyzed but the rocket units are almost always tested to assure that heat is transferred satisfactorily under all operating and emergency conditions. Heat transfer calculations are useful to guide the design, testing, and failure investigations. Those rocket combustion devices that are regeneratively cooled or radiation cooled can reach thermal equilibrium and the steady-state heat transfer relationships will apply. Transient heat transfer conditions apply not only during thrust buildup (starting) and shutdown of all rocket propulsion systems, but also with cooling techniques that never reach equilibrium, such as with ablative materials.

Sophisticated *finite element analysis* (FEA) programs of heat transfer have been available for at least a dozen years and several different FEA computer programs have been used for the analysis of thrust chamber steady-state and transient heat transfer, with different chamber geometries or different materials with temperature variant properties. A detailed description of this powerful analysis is beyond the scope of this book, but can be found in Refs. 8-10 and 8-11. Major rocket propulsion organizations have developed their own ver-

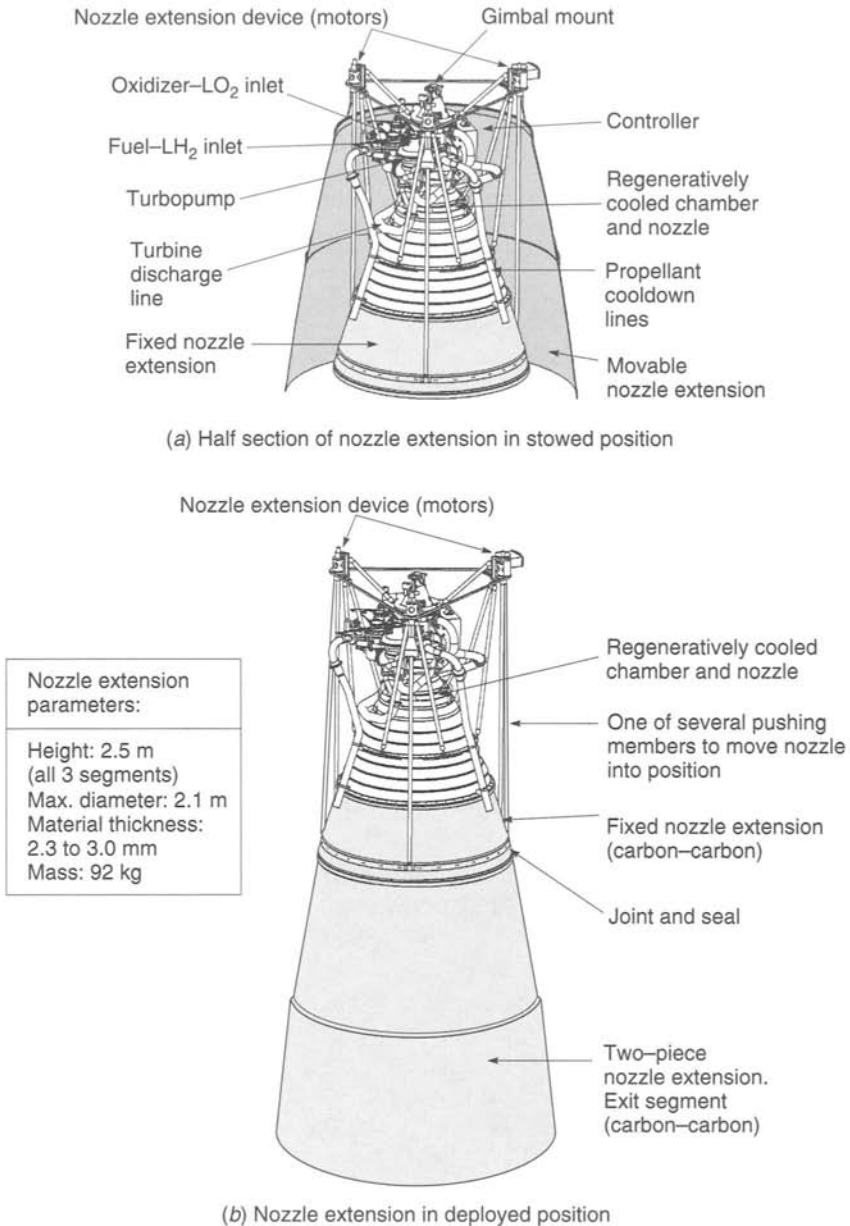


**FIGURE 8-19.** The RL-10B-2 rocket engine has an extendible nozzle cone or skirt, which is placed around the engine during the ascent of the Delta III launch vehicle. This extension is lowered into position by electromechanical devices after the launch vehicle has been separated from the upper stage at high altitude and before firing. (Courtesy of Pratt & Whitney, a division of United Technologies.)

sions of suitable computer programs for solving their heat transfer problems. This section gives the basic relationships that are the foundation for FEA programs. They are intended to give some understanding of the phenomena and underlying principles.

### General Steady-State Heat Transfer Relations

For heat transfer *conduction* the following general relation applies:

$$\frac{Q}{A} = -\kappa \frac{dT}{dL} = -\kappa \frac{\Delta T}{L} \quad (8-14)$$

where  $Q$  is the heat transferred per unit across a surface  $A$ ,  $dT/dL$  the temperature gradient with respect to thickness  $L$  at the surface  $A$ , and  $\kappa$  the thermal conductivity expressed as the amount of heat transferred per unit time through a unit area of surface for 1° temperature difference over a unit wall thickness. The negative sign indicates that temperature decreases as thickness increases.

The steady-state heat transfer through the chamber wall of a liquid-cooled rocket chamber can be treated as a series type, steady-state heat transfer problem with a large temperature gradient across the gaseous film on the inside of the chamber wall, a temperature drop across the wall, and, in cases of cooled chambers, a third temperature drop across the film of the moving cooling fluid. It is a combination of convection at the boundaries of the flowing fluids and conduction through the chamber walls. The problem is basically one of heat and mass transport associated with conduction through a wall. It is shown schematically in Fig. 8-20.

The general steady-state heat transfer equations for regeneratively cooled thrust chambers can be expressed as follows:

$$q = h(T_g - T_l) = Q/A \quad (8-15)$$

$$= \frac{T_g - T_l}{1/h_g + t_w/\kappa + 1/h_l} \quad (8-16)$$

$$= h_g(T_0 - T_{wg}) \quad (8-17)$$

$$= (\kappa/t_w)(T_{wg} - T_{wl}) \quad (8-18)$$

$$= h_l(T_{wl} - T_l) \quad (8-19)$$

where  $q$  is heat transferred per unit area per unit time,  $T_g$  the absolute chamber gas temperature,  $T_l$  the absolute coolant liquid temperature,  $T_{wl}$  the absolute wall temperature on the liquid side of the wall,  $T_{wg}$  the absolute wall temperature on the gas side of the wall,  $h$  the overall film coefficient,  $h_g$  the gas film coefficient,  $h_l$  the coolant liquid film coefficient,  $t_w$  the thickness of the chamber wall, and  $\kappa$  the conductivity of the wall material. The strength and thermal properties of materials are functions of temperature. Any consistent set of units

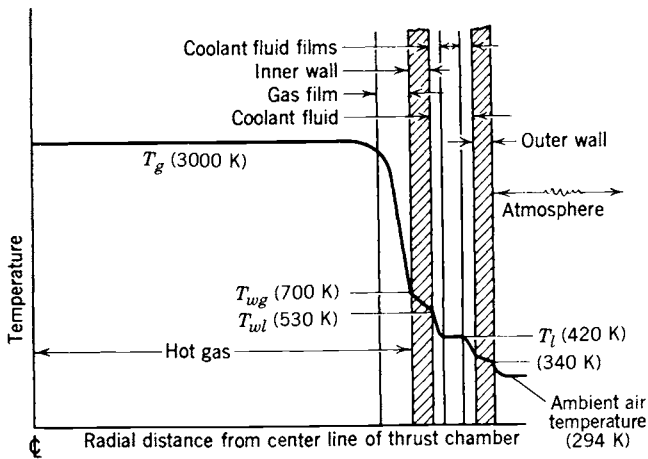


**FIGURE 8-20.** Temperature gradients in cooled rocket thrust chamber. The listed temperatures are typical.

can be used in these equations. These simple relations assume that the heat flow is radial. The simple quasi-one-dimensional theory also often assumes that the thermal conductivity and the film coefficients are at average values and not functions of temperature or pressure. A two- or three-dimensional finite element model would also need to be used to analyze the heat transfer in the axial directions, which usually occurs in the nozzle throat wall regions; some of the heat from the hot nozzle insert is transferred to wall regions upstream and downstream of the insert.

Because the film coefficients, the gas and liquid coolant temperatures, the wall thickness, and the surface areas usually vary with the axial distance within a combustion chamber (assuming axial heat transfer symmetry), the *total heat transfer per unit time*  $Q$  can be found by integrating the local heat transfer over the entire internal surface area of the chamber and the nozzle:

$$Q = \int q \, dA = \pi \int Dq \, dL \quad (8-20)$$

Because both  $q$  and  $D$  are complicated functions of  $L$ , the equation usually has to be solved by dividing the rocket chamber into finite lengths. Assuming that  $q$  is given by Eqs. 8-15 to 8-19 and remains constant over the length of each element gives an approximate solution.

The important quantities for controlling the heat transfer across a rocket chamber wall are the fluid film boundaries established by the combustion products on one side of the wall and the coolant flow on the other. The gas film coefficient largely determines the numerical value of the heat transfer rate, and the liquid film largely determines the value of the wall temperatures. The

determination of the film coefficients in Eqs. 8-17 and 8-19 is difficult because of the complex geometries, the nonuniform velocity profile, the surface roughness, the boundary layer behavior, and the combustion oscillations.

Conventional heat transfer theory is usually given in terms of several dimensionless parameters (Ref. 8-10):

$$\frac{h_g D}{\kappa} = 0.026 \left( \frac{Dv\rho}{\mu} \right)^{0.8} \left( \frac{\mu c_p}{\kappa} \right)^{0.4} \quad (8-21)$$

where  $h_g$  is the film coefficient,  $D$  the diameter of the chamber of the nozzle,  $v$  the calculated average local gas velocity,  $\kappa$  the conductivity of the gas,  $\mu$  the absolute gas viscosity,  $c_p$  the specific heat of the gas at constant pressure, and  $\rho$  the gas density.

In Eq. 8-21 the quantity  $h_g D/\kappa$  is known as the Nusselt number, the quantity  $Dv\rho/\mu$  as the Reynolds number, and the quantity  $c_p \mu/\kappa$  as the Prandtl number  $Pr$ . The gas film coefficient  $h_g$  can be determined from Eq. 8-21:

$$h_g = 0.026 \frac{(\rho v)^{0.8}}{D^{0.2}} Pr^{0.4} \kappa/\mu^{0.8} \quad (8-22)$$

where  $\rho v$  is the local mass velocity, and the constant 0.026 is dimensionless. In order to compensate for some of the boundary layer temperature gradient effects on the various gas properties in rocket combustion, Bartz (Ref. 8-12) has surveyed the agreement between theory and experiment and developed semi-empirical correction factors:

$$h_g = \frac{0.026}{D^{0.2}} \left( \frac{c_p \mu^{0.2}}{Pr^{0.6}} \right) (\rho v)^{0.8} \left( \frac{\rho_{am}}{\rho'} \right) \left( \frac{\mu_{am}}{\mu_0} \right)^{0.2} \quad (8-23)$$

The subscript 0 refers to properties evaluated at the stagnation or combustion temperature; the subscript  $am$  refers to properties at the arithmetic mean temperature of the local free-stream static temperature and the wall temperatures; and  $\rho'$  is the free-stream value of the local gas density. Again, the empirical constant 0.026 is dimensionless when compatible dimensions are used for the other terms. The gas velocity  $v$  is the local free-stream velocity corresponding to the density  $\rho'$ . Since density raised to the 0.8 power is roughly proportional to the pressure and the gas film coefficient is roughly proportional to the heat flux, it follows that the heat transfer rate increases approximately linearly with the chamber pressure. These heat transfer equations have been validated for common propellants, limited chamber pressure ranges, and specific injectors (see Ref. 8-13).

The temperature drop across the inner wall and the maximum temperature are reduced if the wall is thin and is made of material of high thermal con-

ductivity. The wall thickness is determined from strength considerations and thermal stresses, and some designs have as little as 0.025 in. thickness.

Surface roughness can have a large effect on the film coefficients and thus on the heat flux. Measurements have shown that the heat flow can be increased by a factor of up to 2 by surface roughness and to higher factors when designing turbulence-creating obstructions in the cooling channels. Major surface roughness on the gas side will cause the gas locally to come close to stagnation temperature. However, surface roughness on the liquid coolant side of the wall will enhance turbulence and the absorption of heat by the coolant and reduce wall temperatures.

**Example 8-1.** The effects of varying the film coefficients on the heat transfer and the wall temperatures are to be explored. The following data are given:

Wall thickness	0.445 mm
Wall material	Low-carbon steel
Average conductivity	43.24 W/m <sup>2</sup> ·K/m
Average gas temperature	3033 K or 2760°C
Average liquid bulk temperature	311.1 K or 37.8°C
Gas-film coefficient	147 W/m <sup>2</sup> ·°C
Liquid-film coefficient	205,900 W/m <sup>2</sup> ·°C

Vary  $h_g$  (at constant  $h_l$ ), then vary  $h_l$  (at constant  $h_g$ ), and then determine the changes in heat transfer rate and wall temperatures on the liquid and the gas side of the wall.

**SOLUTION.** Use Eqs. 8-16 to 8-19 and solve for  $q$ ,  $T_{wg}$ , and  $T_{wl}$ . The answers shown in Table 8-4 indicate that variations in the gas-film coefficient have a profound influence on the heat transfer rate but relatively little effect on the wall temperature. The exact opposite is true for variations in the liquid-film coefficient; here, changes in  $h_l$  produce little change in  $q$  but a fairly substantial change in the wall temperature.

**TABLE 8-4.** Change in Film Coefficient

Change in Film Coefficient (%)		Change in Heat Transfer (%)	Wall Temperature (K)	
Gas Film	Liquid Film		Gas Side, $T_{wg}$	Liquid Side, $T_{wl}$
50	100	50	324.4	321.1
100	100	100	337.2	330.5
200	100	198	362.8	349.4
400	100	389	415.6	386.1
100	50	99	356.1	349.4
100	25	98	393.3	386.7
100	12.5	95	460.0	397.8
100	6.25	91	596.7	590.5

### Transient Heat Transfer Analysis

An uncooled (high melting point) metal thrust chamber is the simplest type to analyze, because there is no chemical change. Thermal equilibrium is not reached. The uncooled walls act essentially as a heat sponge and absorb heat from the hot gases. With the aid of experimental data to determine some typical coefficients, it is possible in some cases to predict the transient heating of uncooled walls.

Heat is transferred from the hot gases to the wall, and during operation a changing temperature gradient exists across the wall. The heat transferred from the hot wall to the surrounding atmosphere, and by conduction of metal parts to the structure, is negligibly small during this transient heating. Each local point within the wall has its temperature raised as the burning process is extended in time. After the completion of the rocket's operation, the wall temperatures tend to equalize. A typical temperature-time-location history is given in Fig. 8-21. Here the horizontal line at  $T = 21^\circ\text{C}$  denotes the initial

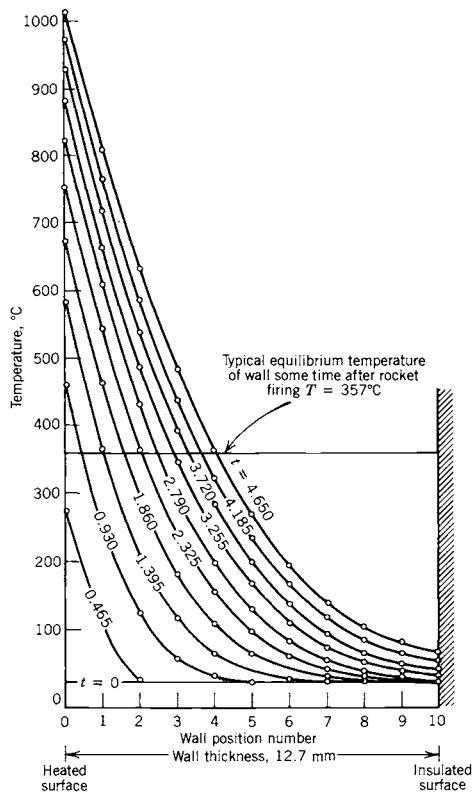


**FIGURE 8-21.** Typical temperature distributions through a wall of an uncooled metal thrust chamber as a function of heating time.

equilibrium condition of the wall before the rocket operates; the various curves show the temperature profile across the wall at successive time intervals after initiation of combustion. The line at  $T = 357^\circ\text{C}$  shows an equilibrium temperature of the wall a finite time after cutoff.

The heat transferred across the hot surface of the wall (and distributed within the wall by conduction) must be less than the heat-absorbing capacity of the wall material below the critical temperature. If heat transfer to the outside atmosphere and axially within the metal wall is neglected, this can be expressed in a very simplified form:

$$Q \Delta t = -\kappa A(dT/dL)\Delta t = m\bar{c}\Delta T \quad (8-24)$$

where  $Q$  is the heat per second transferred across area  $A$ . Eq. 8-17 shows that  $Q/A$  depends on the hot gas temperature, the wall temperature, and the gas film coefficient. The heat conductivity  $\kappa$  depends on the material and its temperature;  $\Delta T$  denotes the average wall temperature increment;  $dT/dL$  the temperature gradient of the heat flow near the hot wall surface in degrees per unit thickness;  $m$  the mass of a unit area of wall;  $\bar{c}$  the average specific heat of the wall material; and  $\Delta t$  at the time increment. The chamber and nozzle walls can be divided into cylindrical or conical segments, and each wall segment in turn is divided into an arbitrary number of axisymmetric concentric layers, each of a finite thickness. At any given time the heat conducted from any one layer of the wall exceeds the heat conducted into the next outer layer by the amount of heat absorbed in raising the temperature of the particular layer. This iterative approach lends itself readily to two- or three-dimensional computer analysis, resulting in data similar to Fig. 8-21. It is usually sufficient to determine the heat transfer at the critical locations, such as in the nozzle throat region.

A more complex three-dimensional analysis can also be undertaken; here the wall geometry is often more complex than merely cylindrical, heat is conducted also in directions other than normal to the axis, temperature variable properties are used, boundary layer characteristics vary with time and location, and there may be more than one material layer in the wall.

A number of mathematical simulations of transient heat transfer in *ablative materials* have been derived, many with limited success. This approach should include simulation for the pyrolysis, chemical decomposition, char depth, and out-gassing effects on film coefficient, and it requires good material property data. Most simulations require some experimental data.

### Steady-State Transfer to Liquids in Cooling Jacket

The term *regenerative cooling* is used for rockets where one of the propellants is circulated through cooling passages around the thrust chamber prior to the injection and burning of this propellant in the chamber. It is really forced convection heat transfer. The term *regenerative* is perhaps not altogether



appropriate here, and it bears little relation to the meaning given to it in steam turbine practice. It is intended to convey the fact that the heat absorbed by the coolant propellant is not wasted but augments its initial temperature and raises its energy level before it passes through the injector. This increase in the internal energy of the liquid propellant can be calculated as a correction to the enthalpy of the propellant (see Chapter 5). However, the overall effect on rocket performance is usually very slight. With some propellants the specific impulse can be 1% larger if the propellants are preheated through a temperature differential of 100 to 200°C. In hydrogen-cooled thrust chambers and in small combustion chambers, where the wall-surface-to-chamber volume ratio is relatively large, the temperature rise in the regenerative coolant will be high, and the resulting increase in specific impulse is sometimes more than 1%.

The behavior of the *liquid film* is critical for controlling the wall temperatures in forced convection cooling of rocket devices at high heat fluxes (see Table 8-4 and Refs. 8-14 and 8-15). At least four different types of film appear to exit, as can be interpreted from Fig. 8-22. Here the heat transfer rate per unit of wall surface is shown as a function of the difference between the wall temperature on the liquid side  $T_{wl}$  and the bulk temperature of the liquid  $T_l$ .

1. The normal *forced convection* region at low heat flux appears to have a liquid boundary layer of predictable characteristics. It is indicated by region  $A-B$  in Fig. 8-22. Here the wall temperature is usually below the boiling point of the liquid at the cooling jacket pressure. In steady-state heat transfer analysis the liquid film coefficient can be approximated by the usual equation (see Refs. 8-10 and 8-12):

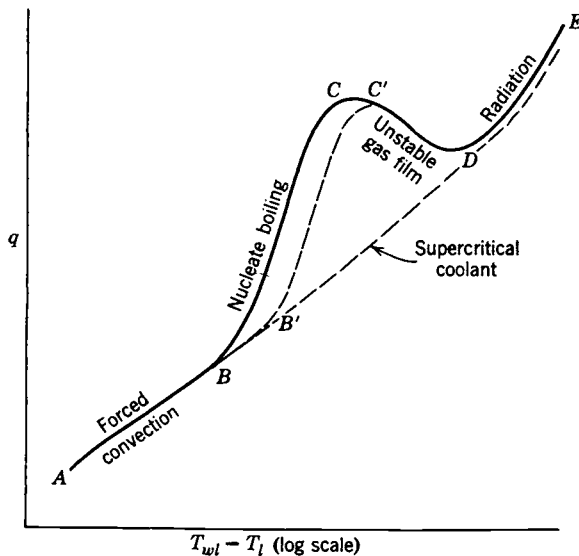


FIGURE 8-22. Regimes in transferring heat from a hot wall to a flowing liquid.

$$h_l = 0.023 \bar{c} \frac{\dot{m}}{A} \left( \frac{Dv\rho}{\mu} \right)^{-0.2} \left( \frac{\mu \bar{c}}{\kappa} \right)^{-2/3} \quad (8-25)$$

where  $\dot{m}$  is the fluid mass flow rate,  $\bar{c}$  its average specific heat,  $A$  the cross-sectional flow area,  $D$  the equivalent diameter of the coolant passage cross section,\*  $v$  the fluid velocity,  $\rho$  the coolant density,  $\mu$  its absolute viscosity, and  $\kappa$  its conductivity. Many liquid-cooled rocket devices operate in this regime of heat transfer. Values of the physical properties of several propellants are given in Tables 8-5 and 7-1. In Table 8-5 it can be seen that hydrazine is a good heat absorber, but kerosene is poor.

2. When the wall temperature  $T_{wl}$  exceeds the boiling point of the liquid by perhaps 10 to 50 K, small vapor bubbles form at the wall surface. These small, nuclei-like bubbles cause local turbulence, break away from the wall, and collapse in the cooler liquid. This phenomenon is known as *nucleate boiling*. The turbulence induced by the bubbles changes the character of the liquid film and, augmented by the vaporization of some of the propellant, the heat transfer rate is increased without a proportional increase in the temperature drop across the film, as can be seen by the steep slope *B-C* of the curve in Figure 8-22. If the pressure of the fluid is raised, then the boiling point is also raised and the nucleate

TABLE 8-5. Heat Transfer Characteristics of Several Liquid Propellants

Liquid Coolant	Boiling Characteristics		Nucleate Boiling Characteristics					
	Pressure (MPa)	Boiling Temp. (K)	Critical Temp. (K)	Critical Pressure (MPa)	Temp. (K)	Pressure (MPa)	Velocity (m/sec)	$q_{\max}$ (MW/m <sup>2</sup> )
Hydrazine	0.101	387	652	14.7	322.2	4.13	10	22.1
	0.689	455					20	29.4
	3.45	540			405.6	4.13	10	14.2
	6.89	588					20	21.2
Kerosene	0.101	490	678	2.0	297.2	0.689	1	2.4
	0.689	603					8.5	6.4
	1.38	651			297.2	1.38	1	2.3
	1.38	651					8.5	6.2
Nitrogen tetroxide	0.101	294	431	10.1	288.9	4.13	20	11.4
	0.689	342			322.2			9.3
	4.13	394			366.7			6.2
Unsymmetrical dimethyl hydrazine	0.101	336	522	6.06	300	2.07	10	4.9
	1.01	400					20	7.2
	3.45	489			300	5.52	10	4.7

\*The grooves, tubes, or coolant passages in liquid propellant rocket chambers are often of complex cross section. The *equivalent diameter*, needed for fluid-film heat transfer calculations, is usually defined as four times the hydraulic radius of the coolant passage; the hydraulic radius is the cross-sectional flow area divided by the wetted perimeter.

boiling region shifts to the right, to  $B'-C'$ . This boiling permits a substantial increase in the heat transfer beyond that predicted by Eq. 8-25. This phenomenon often occurs locally in the nozzle throat area, where the heat flux is high.

3. As the heat transfer is increased further, the rate of bubble formation and the bubble size become so great that the bubbles are unable to escape from the wall rapidly enough. This reaction (shown as  $C-D$  in Fig. 8-22) is characterized by an unstable *gas film* and is difficult to obtain reproducibly in tests. When a film consisting largely or completely of gas forms along the hot wall surface, then this film acts as an insulation layer, causing a decrease in heat flux and, usually, a rapid increase in wall temperature, often resulting in a burnout or melting of the wall material. The maximum feasible heat transfer rate (point  $C$ ) is indicated as  $q_{\max}$  in Table 8-5 and appears to be a function of the cooling-fluid properties, the presence of dissolved gases, the pressure, and the flow velocity.
4. As the temperature difference across the film is further increased, the wall temperatures reach values in which heat transfer by *radiation* becomes important. Region  $D-E$  is not of interest to rocket designers.

Cooling can also be accomplished by a fluid above its critical point with coolants such as hydrogen. In this case there is no nucleate boiling and the heat transfer increases with the temperature difference, as shown by the supercritical (dashed) line in Fig. 8-22. Liquid hydrogen is an excellent coolant, has a high specific heat, and leaves no residues.

Chemical changes in the liquid can seriously influence the heat transfer from hot walls to liquids. Cracking of the fuel, with an attendant formation of insoluble gas, tends to reduce the maximum heat flux and thus promote failure more readily. Hydrocarbon fuel coolants (methane, jet fuel) can break down and form solid, sticky carbon deposits inside the cooling channel, impeding the heat transfer. Other factors influencing steady-state coolant heat transfer are gas radiation to the wall, bends in the coolant passage, improper welds or manufacture, and flow oscillations caused by turbulence or combustion unsteadiness. Some propellants, such as hydrazine, can decompose spontaneously and explode in the cooling passage if they become too hot.

To achieve a good *heat-absorbing capacity of the coolant*, the pressure and the coolant flow velocity are selected so that boiling is permitted locally but the bulk of the coolant does not reach this boiling condition. The total heat rejected by the hot gases to the surface of the hot walls, as given by Eq. 8-15 must be less than that permitted by the temperature rise in the coolant, namely

$$qA = Q = \dot{m}\bar{c}(T_1 - T_2) \quad (8-26)$$

where  $\dot{m}$  is the coolant mass flow rate,  $\bar{c}$  the average specific heat of the liquid,  $T_1$  the initial temperature of the coolant as it enters the cooling jacket, and  $T_2$

its final temperature.  $Q$  is the rate of heat absorption per unit time;  $q$  is this same rate per unit heat transfer area.  $A$ .  $T_2$  should be below the boiling point prevailing at the cooling jacket pressure.

## Radiation

Radiation heat emission is the electromagnetic radiation emitted by a gas, liquid, or solid body by the virtue of its temperature and at the expense of its internal energy. It covers the wavelength range from 10,000 to 0.0001  $\mu\text{m}$ , which includes the visible range of 0.39 to 0.78  $\mu\text{m}$ . Radiation heat transfer occurs most efficiently in a vacuum because there is no absorption by the intervening fluids.

The heat transmitted by the mechanism of radiation depends primarily on the temperature of the radiating body and its surface condition. The second law of thermodynamics can be used to prove that the radiant energy  $E$  is a function of the fourth power of the absolute temperature  $T$ :

$$E = f\epsilon\sigma AT^4 \quad (8-27)$$

The energy  $E$  radiated by a body is defined as a function of the emissivity  $\epsilon$ , which is a dimensionless factor for surface condition and material properties, the Stefan-Boltzmann constant  $\sigma$  ( $5.67 \times 10^{-8} \text{ W/m}^2\text{-K}^4$ ), the surface area  $A$ , the absolute temperature  $T$ , and the geometric factor  $f$ , which depends on the arrangement of adjacent parts and the shape. At low temperatures (below 800 K) radiation accounts for only a negligible portion of the total heat transfer in a rocket device and can usually be neglected.

In rocket propulsion there are these radiation concerns:

1. Emission of hot gases to the internal walls of a combustion chamber, a solid propellant grain, a hybrid propellant grain or a nozzle.
2. Emission to the surroundings or to space from the external surfaces of hot hardware (radiation-cooled chambers, nozzles, or electrodes in electric propulsion).
3. Radiation from the hot plume downstream of the nozzle exit. This is described in Chapter 18.

In rocket combustion devices gas temperatures are between 1900 and 3900 K or about 3000 to 6600°F; their radiation contributes between 3 and 40% of the heat transfer to the chamber walls, depending on the reaction gas composition, chamber size, geometry, and temperature. It can be a significant portion of the total heat transfer. In solid propellant motors the radiation heating of the grain surfaces can be critical to the burning rate, as discussed in Chapter 13. The absorption of radiation on the wall follows essentially the same laws as those of emission. Metal surfaces and formed tubes reflect much of the radiant energy, whereas ablative materials and solid propellant seem to absorb most of

the incident radiation. A highly reflective surface on the inside wall of a combustor tends to reduce absorption and to minimize the temperature increase of the walls.

The hot reaction gases in rocket combustion chambers are potent radiation sources. Gases with symmetrical molecules, such as hydrogen, oxygen, and nitrogen, have been found not to show many strong emission bands in those wavelength regions of importance in radiant heat transfer. Also, they do not really absorb much radiation and do not contribute considerable energy to the heat transfer. Heteropolar gases, such as water vapor, carbon monoxide, carbon dioxide, hydrogen chloride, hydrocarbons, ammonia, oxides of nitrogen, and the alcohols, have strong emission bands of known wavelengths. The radiation of energy of these molecules is associated with the quantum changes in their energy levels of rotation and interatomic vibration. In general, the radiation intensity of all gases increases with their volume, partial pressure, and the fourth power of their absolute temperature. For small thrust chambers and low chamber pressures, radiation contributes only a small amount of energy to the overall heat transfer.

If the hot reaction gases contain small solid particles or liquid droplets, then the radiation heat transfer can increase dramatically by a factor of 2 to 10. The particulates greatly increase the radiant energy as explained in Section 18.1. For example, the reaction gas from some slurry liquid propellants and many solid propellants contains fine aluminum powder. When burned to form aluminum oxide, the heat of combustion and the combustion temperature are increased (raising heat transfer), and the specific impulse is raised somewhat (giving improved performance). The oxide can be in the form of liquid droplets (in the chamber) or solid particles (in the nozzle diverging section), depending on the local gas temperature. Furthermore, the impact of these particulates with the wall will cause an additional increase in heat transfer, particularly to the walls in the nozzle throat and immediately upstream of the nozzle throat region. The particles also cause erosion or abrasion of the walls.

## 8.4. STARTING AND IGNITION

The starting of a thrust chamber has to be controlled so that a timely and even ignition of propellants is achieved and the flow and thrust are built up smoothly and quickly to their rated value (see Ref. 6-1). The *initial propellant flow* is less than *full flow*, and the *starting mixture ratio* is usually different from the *operating mixture ratio*. A low initial flow prevents an excessive accumulation of unignited propellants in the chamber.

The starting injection velocity is low, the initial vaporization, atomization, and mixing of propellants in a cold combustion chamber is incomplete, and there are local regions of lean and rich mixtures. With cryogenic propellants the initial chamber temperature can be below ambient. The optimum starting mixture is therefore only an average of a range of mixture ratios, all of which

should be readily ignited. Mixture ratios near the stoichiometric mixture ratio have a high heat release per unit of propellant mass and therefore permit bringing the chamber and the gases up to equilibrium faster than would be possible with other mixtures. The operating mixture ratio is usually fuel rich and is selected for optimum specific impulse. One method of analytical modeling of the ignition of cryogenic propellants is given in Ref. 8–16.

The *time delay for starting* a thrust chamber ideally consists of the following time periods:

- (1) time needed to fully open the propellant valves (typically 0.002 to more than 1.00 sec, depending on valve type and its size and upstream pressure);
- (2) time needed to fill the liquid passage volume between the valve seat and the injector face (piping, internal injector feed holes, and cavities);
- (3) time for forming discrete streams or jets of liquid propellant (sometimes gaseous propellant, if cryogenic liquid is preheated by heat of ambient temperature cooling jacket) and for initial atomization into small droplets and for mixing these droplets;
- (4) time needed for droplets to vaporize and ignite (laboratory tests show this to be very short, 0.02 to 0.05 sec, but this depends on the propellants and the available heat);
- (5) once ignition is achieved at a particular location in the chamber, it takes time to spread the flame or to heat all the mixed propellant that has entered into the chamber, to vaporize it, and to raise it to ignition temperature;
- (6) time needed to raise the chamber to the point where combustion will be self sustaining, and then to its full pressure.

There are overlaps in these delays and several of them can occur simultaneously. The delays [items (1), (2), (3), (5), and (6) above] are longer with large injectors or large diameter chambers. Small thrusters can usually be started very quickly, in a few milliseconds, while larger units require 1 sec or more.

In starting a thrust chamber one propellant always reaches the chamber a short time ahead of the other; it is almost impossible to synchronize exactly the fuel and oxidizer feed systems so that the propellants reach the chamber simultaneously at all injection holes. Frequently, a more reliable ignition is assured when one of the propellants is intentionally made to reach the chamber first. For example, for a fuel-rich starting mixture the fuel is admitted first. Reference 8–17 describes the control of the propellant lead.

Other factors influencing the starting flows, the propellant lead or lag, and some of the delays mentioned above are the liquid pressures supplied to the injector (e.g., regulated pressure), the temperature of the propellant (some can be close to their vapor point), and the amount of insoluble gas (air bubbles) mixed with the initial quantity of propellants.

The propellant valves (and the flow passages between them and the injector face) are often so designed that they operate in a definite sequence, thereby assuring an intentional lead of one of the propellants and a controlled buildup of flow and mixture ratio. Often the valves are only partially opened, avoiding an accumulation of hazardous unburned propellant mixture in the chamber. Once combustion is established, the valves are fully opened and full flow may reach the thrust chamber assembly. The initial reduced flow burning period is called the *preliminary stage*. Section 10.5 describes the starting controls.

Full flow in the larger thrust chambers is not initiated with non-self-igniting propellants until the controller received a signal of successful ignition. The verification of ignition or initial burning is often built into engine controls using visual detection (photocell), heat detection (pyrometer), a fusible wire link, or sensing of a pressure rise. If the starting controls are not designed properly, unburnt propellant may accumulate in the chamber; upon ignition it may then explode, causing sometimes severe damage to the rocket engine. Starting controls and engine flow calibrations are discussed in Section 10.5

Non-spontaneously ignitable propellants need to be activated by absorbing energy prior to combustion initiation. This energy is supplied by the *ignition system*. Once ignition has begun the flame is self-supporting. The igniter has to be located near the injector in such a manner that a satisfactory starting mixture at low initial flow is present at the time of igniter activation, yet it should not hinder or obstruct the steady-state combustion process. At least five different types of successful propellant ignition systems have been used.

*Spark plug ignition* has been used successfully on liquid oxygen–gasoline and on oxygen–hydrogen thrust chambers, particularly for multiple starts during flight. The spark plug is often built into the injector, as shown in Fig. 9–6.

*Ignition by electrically heated wires* has been accomplished, but at times has proven to be less reliable than spark ignition for liquid propellants.

*Pyrotechnic ignition* uses a solid propellant squib or grain of a few seconds' burning duration. The solid propellant charge is electrically ignited and burns with a hot flame within the combustion chamber. Almost all solid propellant rockets and many liquid rocket chambers are ignited in this fashion. The igniter container may be designed to fit directly onto the injector or the chamber (see Fig. 8–1), or may be held in the chamber from outside through the nozzle. This ignition method can only be used once; thereafter the charge has to be replaced.

In *precombustion chamber ignition* a small chamber is built next to the main combustion chamber and connected through an orifice; this is similar to the precombustion chamber used in some internal combustion engines. A small amount of fuel and oxidizer is injected into the precombustion chamber and ignited. The burning mixture enters the main combustion chamber in a torch-like fashion and ignites the larger main propellant flow which is injected into the main chamber. This ignition procedure permits repeated starting of variable-thrust engines and has proved successful with the liquid oxygen–gasoline and oxygen–hydrogen thrust chambers.

*Auxiliary fluid ignition* is a method whereby some liquid or gas, in addition to the regular fuel and oxidizer, is injected into the combustion chamber for a very short period during the starting operation. This fluid is hypergolic, which means it produces spontaneous combustion with either the fuel or the oxidizer. The combustion of nitric acid and some organic fuels can, for instance, be initiated by the introduction of a small quantity of hydrazine or aniline at the beginning of the rocket operation. Liquids that ignite with air (zinc diethyl or aluminum triethyl), when preloaded in the fuel piping, can accomplish a hypergolic ignition. The flow diagram of the RD 170 Russian rocket engine in Fig. 10-10 shows several cylindrical containers prefilled with a hypergolic liquid, one for each of the high pressure fuel supply lines; this hypergolic liquid is pushed out (by the initial fuel) into the thrust chambers and into the pre-burners to start their ignitions.

In vehicles with multiple engines or thrust chambers it is required to start two or more together. It is often difficult to get exactly simultaneous starts. Usually the passage or manifold volumes of each thrust chamber and their respective values are designed to be the same. The temperature of the initial propellant fed to each thrust chamber and the lead time of the first quantity of propellant entering into the chambers have to be controlled. This is needed, for example, in two small thrusters when used to apply roll torques to a vehicle. It is also one of the reasons why large space launch vehicles are not released from their launch facility until there is assurance that all the thrust chambers are started and operating.

## 8.5. VARIABLE THRUST

Section 3.8 mentions the equations related to this topic. One of the advantages of liquid propellant rocket engines is the ability to throttle or to randomly vary the thrust over a wide range. Deep throttling over a thrust range of more than 10:1 is required for relatively few applications. Moon landing, interceptor missiles, and gas generators with variable power output are examples. Moderate throttling (a thrust range of up to perhaps 2.5:1) is needed for trajectory velocity control (as in some tactical missiles), space maneuvers, or temporarily limiting the vehicle velocity (to avoid excessive aerodynamic heating during the ascent through the atmosphere), as in the Space Shuttle main engine.

Throttling is accomplished by reducing the propellant flow supply to the thrust chamber and thus reducing the chamber pressure. The pressure drop in the injector is related to the injection velocity by Eq. 8-5. The accompanying reduction of the injector pressure drop can lead to a very low liquid injection velocity and, thus, to poor propellant mixing, improper stream impingement patterns, and poor atomization, which in turn can lead to lower combustion efficiency and thus lower performance and sometimes unstable combustion.



The variation of flow through a given set of injection orifices and of thrust by this method is limited.

There are several throttling methods whereby the injection pressure drop is not decreased unduly. This permits a change in chamber pressure without a major decrease in injector pressure drop. A moving sleeve mechanism for adjusting the fuel and the oxidizer injection circular sheet spray areas is shown in Fig. 8-3.

One way of preventing unstable operation and a drop-off in performance is to use *multiple thrust chambers* or *multiple rocket engines*, each of which operates always at or near rated conditions. The thrust is varied by turning individual thrust chambers on or off and by throttling all of them over a relatively narrow range.

For small reaction control thrusters the average thrust is usually reduced by pulsing. It is accomplished by controlling the number of cycles or pulses (each has one short fixed-duration thrust pulse plus a short fixed-duration zero-thrust pause), by modulating the duration of individual pulses (with short pauses between pulses), or alternatively by lengthening the pause between pulses.

## 8.6. SAMPLE THRUST CHAMBER DESIGN ANALYSIS

This example shows how a thrust chamber is strongly influenced by the overall vehicle system requirements or the mission parameters and the vehicle design. As outlined in the Design Section of Chapter 10 and in the discussion of the selection of propulsion systems in Chapter 17, each engine goes through a series of rationalizations and requirements that define its key parameters and its design. In this example we describe how the thrust chamber parameters are derived from the vehicle and engine requirements. The overall system requirements relate to the mission, its purpose, environment, trajectories, reusability, reliability, and to restraints such as allowable engine mass, or maximum dimensional envelope. We are listing some, but not all of the requirements. It shows how theory is blended with experience to arrive at the initial choices of the design parameters.

Here we define the application as a new upper stage of an existing multistage space launch vehicle, that will propel a payload into deep space. This means continuous firing (no restart or reuse), operating in the vacuum of space (high nozzle area ratio), modest acceleration (not to exceed  $5 g_0$ ), low cost, moderately high performance (specific impulse), and a thrust whose magnitude depends on the payloads, the flight path and acceleration limits. The desired mission velocity increase of the stage is 3400 m/sec. The engine is attached to its own stage, which is subsequently disconnected and dropped from the payload stage. The payload stage (3500 kg) consists of a payload of 1500 kg (for scientific instruments, power supply, or communications and flight control equipment) and its own propulsion systems (including propellant) of 2000 kg

(for trajectory changes, station keeping, attitude control, or emergency maneuvers). There are two geometric restraints: the vehicle has an outside diameter of 2.0 m, but when the structure, conduits, certain equipment, thermal insulation, fittings, and assembly are considered, it really is only about 1.90 m. The restraint on the stage length of 4.50 m maximum will affect the length of the thrust chamber. We can summarize the key requirements:

Application	Uppermost stage to an existing multistage launch vehicle
Payload	3500 kg
Desired velocity increase $\Delta u$	3400 m/sec in gravity free vacuum
Maximum stage diameter	1.90 m
Maximum stage length	4.50 m
Maximum acceleration	5 $g_0$

**Decisions on Basic Parameters.** The following engine design decisions or parameter selection should be made early in the design process:

- Propellant combination
- Chamber pressure
- Nozzle area ratio
- Feed system, using pumps or pressurized tanks
- Thrust level

From a performance point of view, the best *propellant combination* would be liquid oxygen with liquid hydrogen. However, this bipropellant would have a low average specific gravity (0.36), a very large liquid hydrogen tank, and would cause an increase in vehicle drag during ascent. It would have some potential problems with exceeding the allocated stage volume, hydrogen mass losses, and the vehicle structure. The lower stages of the existing launch vehicle use liquid oxygen with RP-1 fuel with an average specific gravity of about 1.014, and the launch pad is already equipped for supplying these. The new stage is limited in volume and cross section. Because of these factors the propellant combination of liquid oxygen and RP-1 (a type of kerosene) is selected. From Fig. 5-1 we see that the theoretical specific impulse is between 280 and 300 sec, depending on the mixture ratio and whether we use frozen or shifting chemical equilibrium in the nozzle flow expansion. This figure also shows that the maximum value of the characteristic velocity  $c^*$  is reached at a mixture ratio of about 2.30, which is a fuel-rich mixture. We select this mixture ratio. Its combustion temperature is lower than the mixture ratios with higher values, and this should make the cooling of the thrust chamber easier. We will see later that cooling may present some problems. Based on universal experience, we select a value of  $I_s$  part way (about 40%) between the values for frozen and shifting equilibrium, namely 292 sec at the standard chamber pressure of 1000 psi or 6.895 MPa, and a nozzle big enough for expansion to sea level. From Fig. 5-1 and Table 5-5 we find the molecular

mass to be 23 kg/kg-mol and the specific heat ratio  $k$  to be about 1.24. Later we will correct this value of  $I_s$  from this standard reference condition to the actual vacuum specific impulse of the thrust chamber.

Next we will select a chamber pressure, a nozzle area ratio and a feed system concept. Historically there has been favorable experience with this propellant combination at chamber pressures between 400 and 3400 psia with nozzle area ratios up to about 40 with both gas generator cycles and staged combustion cycles, giving proof that this is feasible. The following considerations enter into this selection:

1. Higher chamber pressures allow a smaller thrust chamber and (for the same nozzle exit pressure) a shorter nozzle cone with a smaller nozzle exit diameter. The thrust chamber is small enough for a toroidal tank to be built around it, and this conserves stage length. This not only saves vehicle space, but usually also some inert mass in the vehicle and the engine. Figure 8-23 shows the relative sizes of thrust chambers for three chamber pressures and two nozzle area ratios ( $\epsilon$  of 100 and 300). The nozzle length and exit diameter cannot exceed the values given in the requirements, which, as can be seen, rules out low chamber pressure or high area ratio. The dimensions shown are calculated later in this analysis.

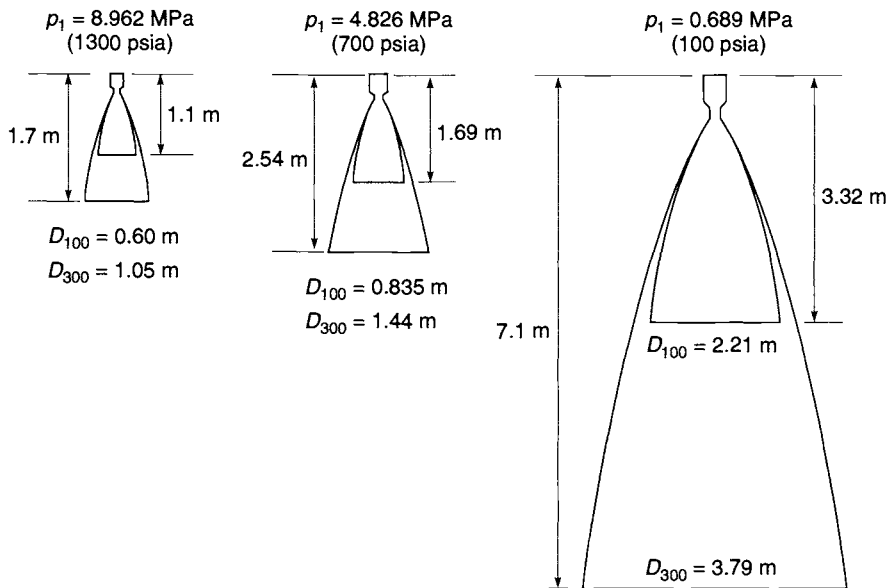


**FIGURE 8-23.** Comparison of thrust chamber sizes for three chamber pressures and two nozzle area ratios (100 and 300).

2. The heat transfer rate is almost proportional to the gas density, which is proportional to the chamber pressure, as shown by Eq. 8-21 and 8-23. On some prior thrust chambers there have been problems with the formation of solid carbon layer or deposits either inside the cooling jacket (increasing wall temperatures) or on the inner walls of the combustion chamber (the solid can flake off and cause burnout). This favors a lower chamber pressure.
3. Concern over leak-free seals for both static and dynamic seal increases with chamber pressure, which in turn causes all feed pressures also to increase.
4. A feed system using pressurized gas is feasible, but its inert masses of tanks and engine are favorable only, if the chamber pressure is very low, perhaps around 100 psia or less. The tanks for propellants and pressurizing gas become very heavy and the thrust chamber will be very large and exceed the dimensional restraints mentioned above. We therefore cannot use this feed system or very low chamber pressures.
5. If we use a pump feed system, the power needed to drive the pumps increases directly with chamber pressure  $p_1$ . In a gas generator engine cycle this means a slightly reduced performance as the value of  $p_1$  goes up. For a staged combustion cycle it means high pressures, particularly high pressure hot gas flexible piping, and a more complex, heavier, and expensive engine. We therefore select a gas generator cycle (see Fig. 1-4) at a low enough chamber pressure, so that the thrust chamber (and the other inert hardware) will just fit the geometrical constraints, and the engine inert mass and the heat transfer will be reasonable.

For these reasons we pick a *chamber pressure* of 700 psia or 4.825 MPa and an *area ratio* of 100. With further analysis we could have picked  $p_1$  more precisely; it could be somewhat lower or higher. Next we correct the *specific impulse* to the operating conditions using a ratio of thrust coefficients. We can use Eq. 3-30 or interpolate between Figs. 3-7 and 3-8 for a value of  $k = 1.24$ . The reference or standard condition (see Fig. 3-6) is for a pressure ratio  $p_1/p_3$  of  $1000/14.7 = 68$ , which corresponds to an area ratio of about 8. Then  $(C_F)_{\text{standard}} = 1.58$ . For the actual high-altitude operation the pressure ratio is close to infinity and the nozzle has an area ratio of 100; we can determine the thrust coefficient by interpolating  $k = 1.24$ . The result is  $(C_F)_{\text{vacuum}} = 1.90$ . The new ideal specific impulse value for a chamber threshold of 700 psia and a nozzle area ratio of 100 is therefore  $292 \times (1.90/1.58) = 351.1$  sec. In order to correct for losses (divergence, boundary layer, incomplete combustion, some film cooling, etc.) we use a correction factor of 0.96 giving a thrust chamber specific impulse of 337.1 sec. The engine uses a gas generator and this will reduce the engine specific impulse further by a factor of 0.98 or  $(I_s)_{\text{engine}} = 330.3$  sec or an effective exhaust velocity of 3237 m/sec.

**Stage Masses and Thrust Level.** An estimate of the stage masses will next be made. We assume that the inert hardware (tanks, gas, generator, turbopumps, etc.) is about 7% of the propellant mass, which is conservative when compared to existing engines. In a full-fledged engine design this number would be verified or corrected once an estimated mass budget becomes available. From Eq. 4-7

$$e^{\Delta u/v} = \frac{m_o}{m_f} = \frac{m_p + 0.07m_p + 3500}{0.07m_p + 3500} = e^{3400/3237}$$

Solve for  $m_p = 7639$  kg. The final and initial masses of the stage are then 4023 kg and 11,002 kg respectively.

The maximum *thrust* is limited by the maximum allowed acceleration of  $5g_0$ . It is  $F_{\max} = m_0 a = 11,002 \times 5 \times 9.8 = 539,100$  N. This would become a relatively large and heavy thrust chamber. Considerable saving in inert mass can be obtained if a smaller thrust size (but longer firing duration) is chosen. Since this same thrust chamber is going to be used for another mission where an acceleration of somewhat less than  $1.0g_0$  is wanted, a thrust level of 50,000 N or 11,240 lbf is chosen. The maximum acceleration of the stage occurs just before cutoff; it is  $a = F/m_f = 50,000/4023 = 12.4$  m/sec<sup>2</sup> or about 1.26 times the acceleration of gravity. This fits the thrust requirements.

The following have now been determined:

Propellant	Liquid oxygen and liquid kerosene (RP-1)
Mixture ratio (O/F)	2.30 (engine)
Thrust	50,000 N or 11,240 lbf
Chamber pressure	700 psia or 4.826 MPa
Nozzle area ratio	100
Specific impulse (engine)	330.3 sec
Specific impulse (thrust chamber)	337.1 sec
Engine cycle	Gas generator
Usable propellant mass	7478 kg

**Propellant Flows and Dimensions of Thrust Chamber.** From Eq. 2-6 we obtain the propellant mass flow

$$\dot{m} = F/c = 50,000/3200 = 15.625 \text{ kg/sec}$$

When this total flow and the overall mixture ratio are known, then the fuel flow  $\dot{m}_f$  and oxidizer flow  $\dot{m}_o$  for the engine, its gas generator, and its thrust chamber can be determined from Eqs. 6-3 and 6-4 as shown below.

$$\dot{m}_f = \dot{m}/(r + 1) = 15.446/(2.3 + 1) = 4.680 \text{ kg/sec}$$

$$\dot{m}_o = \dot{m}r/(r + 1) = (15.446 \times 2.30)/3.30 = 10.765 \text{ kg/sec}$$

The gas generator flow  $\dot{m}_{gg}$  consumes about 2.0% of the total flow and operates at a fuel-rich mixture ratio of 0.055; this results in a gas temperature of about 890 K.

$$(\dot{m}_f)_{gg} = 0.2928 \text{ kg/sec} \qquad (\dot{m}_o)_{gg} = 0.0161 \text{ kg/sec}$$

The flows through the thrust chamber are equal to the total flow diminished by the gas generator flow, which is roughly 98.0% of the total flow or 15.137 kg/sec.

$$(\dot{m}_f)_{tc} = 4.387 \text{ kg/sec} \qquad (\dot{m}_o)_{tc} = 10.749 \text{ kg/sec}$$

The *duration* is the total effective propellant mass divided by the mass flow rate

$$t_b = m_p/\dot{m}_p = 7478/15.446 = 484.1 \text{ sec or a little longer than 8 minutes}$$

The *nozzle throat area* is determined from Eq. 3-31.

$$A_t = F/(p_1 C_F) = 50,000/(4.826 \times 10^6 \times 1.90) = 0.005453 \text{ m}^2 \text{ or } 54.53 \text{ cm}^2$$

The *nozzle throat diameter* is  $D_t = 8.326 \text{ cm}$ . The internal diameter of the nozzle at exit  $A_2$  is determined from the area ratio of 100 to be  $D_2 = \sqrt{100} \times D_t$  or 83.26 cm. A shortened or *truncated bell nozzle* (as discussed in Section 3.4) will be used with 80% of the length of a  $15^\circ$  conical nozzle, but with the same performance as a  $15^\circ$  cone. The nozzle length (from the throat to the exit) can be determined by an accurate layout or by  $L = (D_2 - D_t)/(2 \tan 15)$  as 139.8 cm. For an 80% shortened bell nozzle this length would be about 111.8 cm. The contour or shape of a shortened bell nozzle can be approximated by a parabola (parabola equation is  $y^2 = 2px$ ). Using an analysis (similar to the analysis that resulted in Fig. 3-14) the maximum angle of the diverging section at the inflection point would be about  $\theta_i = 34^\circ$  and the nozzle exit angle  $\theta_e = 7^\circ$ . The approximate contour consists of a short segment of radius  $0.4r_t$  of a  $34^\circ$  included angle (between points T and I in Fig. 3-14) and a parabola with two known points at I and E. Knowing the tangent angles ( $34$  and  $7^\circ$ ) and the  $y$  coordinates [ $y_e = r_2$  and  $y_i = r_t + 0.382 r_t (1 - \cos \theta_i)$ ] allows the determination of the parabola by geometric analysis. Before detail design is undertaken, a more accurate contour, using the method of characteristics, is suggested.

The *chamber diameter* should be about twice the nozzle throat diameter to avoid pressure losses in the combustion chamber ( $D_c = 16.64 \text{ cm}$ ). Using the approximate length of prior successful smaller chambers and a characteristic length  $L^*$  of about 1.1 m, the chamber length (together with the converging nozzle section) is about 11.8 inch or 29.9 cm. The overall length of the thrust

chamber (169 cm) is the sum of the nozzle length (111.8 cm), chamber (29.9 cm), injector thickness (estimated at 8 cm), mounted valves (estimated at 10 cm), a support structure, and possibly also a gimbal joint. The middle sketch of the three thrust chambers in Fig. 8-23 corresponds roughly to these numbers.

We have now the stage masses, propellant flows, nozzle and chamber configuration. Since this example is aimed at a thrust chamber, data on other engine components or parameters are given only if they relate directly to the thrust chamber or its parameters.

Next we check if there is enough available vehicle volume (1.90 m diameter and 4.50 m long) to allow making a larger nozzle area ratio and thus gain a little more performance. First we determine how much of this volume is occupied by propellant tanks and how much might be left over or be available for the thrust chamber. This analysis would normally be done by tank design specialists. The average density of the propellant mixture can be determined from Eq. 7-1 to be  $1014 \text{ kg/m}^3$  and the total usable propellant of 7478 kg. Using densities from Table 7-1 the fuel volume and the oxidizer volume can be calculated to be 2.797 and  $4.571 \text{ m}^3$  respectively. For a diameter of 1.90 m, a nearly spherical fuel tank, a separate oxidizer cylindrical tank with elliptical ends, 6% ullage, and 2% residual propellant, a layout would show an overall tank length of about 3.6 m in a space that is limited to 4.50 m. This would leave only 0.9 m for the length of the thrust chamber, and this is not long enough. Therefore we would need to resort to a more compact tank arrangement, such as using a common bulkhead between the two tanks or building a toroidal tank around the engine. It is not the aim to design the tanks in this example, but the conclusion affects the thrust chamber. Since the available volume of the vehicle is limited, it is not a good idea to try to make the thrust chamber bigger.

This diversion into the tank design shows how a vehicle parameter affects the thrust chamber design. For example, if the tank design would turn out to be difficult or the tanks would become too heavy, then one of these thrust chamber options can be considered: (1) go to a higher chamber pressure (makes the thrust chamber and nozzle smaller, but heavier), (2) go to a lower thrust engine (will be smaller and lighter), (3) store the nozzle of the upper stage thrust chamber in two pieces and assemble them once the lower stages have been used and discarded (see Fig. 8-19; it is more complex and somewhat heavier), or (4) use more than one thrust chamber in the engine (will be heavier, but shorter). We will not pursue these or other options here.

**Heat Transfer.** The particular computer program for estimating heat transfer and cooling parameters of thrust chambers will depend on the background and experience of specific engineers and rocket organizations. Typical computer programs divide the internal wall surface of the chamber and nozzle into axial incremental axial steps. Usually in a preliminary analysis the heat transfer is estimated only for critical locations such as for the throat and perhaps the chamber.

From Fig. 5-1 and Eq. 3-12 or 3-22 we determine the following gas temperatures for the chamber, nozzle throat region, and a location in the diverging exit section. They are:  $T_1 = 3600$  K,  $T_t = 3243$  K, and  $T_e = 1730$  K at an area ratio of 6.0 in the diverging nozzle section. The chamber and nozzle down to an exit area ratio of 6 will have to be cooled by fuel. For this propellant combination and for the elevated wall temperatures a stainless steel has been successfully used for the inner wall material.

Notice that beyond this area ratio of about 6, the nozzle free stream gas temperatures are relatively low. Uncooled high temperature metals can be used here in this outer nozzle region. Radiation cooling, using a material such as niobium (coated to prevent excessive oxidation) or carbon fibers in a nonporous carbon matrix, is suitable between an area ratio of 6 and about 25. For the final large nozzle exit section, where the temperatures are even lower, a lower cost material such as stainless steel or titanium is suggested. Ablative materials have been ruled out, because of the long duration and the aggressive ingredients in the exhaust gas. The gas compositions of Figs. 5-2 and 5-3 indicate that some free oxygen and hydroxyl is present.

We now have identified the likely materials for key chamber components. The best way to cool the radiation cooled exit segment of the nozzle (beyond area ratio of 6) is to let it stick out of the vehicle structure; the heat can then be freely radiated to space. One way to accomplish this, is to discard the vehicle structure around the nozzle end.

As in Fig. 8-8, the maximum heat transfer rate will be at the nozzle throat region. A variety of heat transfer analysis programs are available for estimating this heat transfer. If a suitable computer program is not available, then an approximate steady-state heat transfer analysis can be made using Eqs. 8-15 to 8-19 and the physical properties (specific heat, thermal conductivity, and density) of RP-1 at elevated temperatures. The film coefficients of Eqs. 8-23 and 8-25 are also needed. This is not done in this example, in part because data tables for the physical properties would take up a lot of space and results are not always reliable. Data from prior thrust chambers with the same propellants indicate a heat transfer rate at the nozzle throat region exceeding  $10 \text{ Btu/in.}^2\text{-sec}$  or  $1.63 \times 10^7 \text{ W/m}^2$ .

The RP-1 fuel is an unusual coolant, since it does not have a distinct boiling point. Its composition is not consistent and depends on the oil stock from which it was refined and the refining process. It is distilled or evaporated gradually over a range of temperatures. The very hot wall can cause the RP-1 to locally break down into carbon-rich material and to partially evaporate or gasify. As long as the small vapor bubbles are recondensed when they are mixed with the cooler portions of the coolant flow, a steady heat transfer process will occur. If the heat transfer is high enough, then these bubbles will not be condensed, may contain noncondensable gases, and the flow will contain substantial gas bubbles and become unsteady, causing local overheating. The recondensing is aided by high cooling passage velocities (more than  $10 \text{ m/sec}$  at the throat region) and by turbulence in these passages. A coolant



flow velocity of 15 m/sec is selected for the throat and 7 m/sec in the chamber and nozzle exit segment.

The material for the cooling jacket will be stainless steel to resist the oxidation and erosion of the fast moving, aggressive hot gas, which contains free oxygen and hydroxyl species. The cooling by fuel will assure that the temperatures of this stainless steel are well below its softening temperature of about 1050 K.

The construction of the cooling jacket can be tubular, as shown in Figs. 8-1 and 8-9, or it can consist of milled channels as shown in Figs. 8-2 and 8-17. The cross section of each tube or cooling channel will be a minimum at the throat region, gradually become larger, and be about two or more times as large at the chamber and diverging nozzle regions. The wall thickness (on the hot gas side) should be as small as possible to reduce the temperature drop across the wall (which reduces the thermal stresses and allows a lower wall temperature) and to minimize the yielding of the material that occurs due to thermal deformation and pressure loads. Figure 8-12 shows this behavior, but for a thick wall. Practical considerations such as manufacturability, the number of test firings before flight, the deformation under pressure loads, the temperature gradient and dimensional tolerances also enter into the selection of the wall thickness. A thickness of 0.5 mm and a cooling velocity of 15 m/sec have been selected for the throat region of the cooling jacket and cooling velocities of 7 m/sec in the chamber and the cooled nozzle segment. Milled slots (rather than tubes) have been selected for this thrust chamber.

The selection of the number of milled slots, their cross sections, and the wall thickness is a function of the coolant mass flow, its pressure, wall stresses, wall material, and the shape of the channel. Figure 8-24 and Table 8-6 describe the channel width and height for different numbers of channels and different locations. The fuel coolant flow is diminished by the gas generator fuel flow (0.293 kg/sec) and is about 4.387 kg/sec. For this flow and a cooling velocity of 15 m/sec in the throat region the cumulative cross-sectional area of all the channels is only about 3.62 cm<sup>2</sup>. The cooling velocity is lower in the chamber and nozzle regions and the cumulative channel flow area will be larger there. The variables are the number of channels, the thickness of the hot wall, the rib thickness between channels, the cooling velocity, the gas temperature, and the

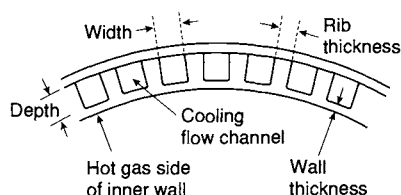


**FIGURE 8-24.** Segment of cooling jacket with milled channels and an electroformed outer wall.

**TABLE 8-6.** Alternative Milled Channel Configurations for Fuel (cooling) Flow of 4.387 kg/sec

<i>Throat Section</i>			<i>Chamber Section</i>		
Wall thickness	0.05 cm		Wall thickness	0.06 cm	
Rib thickness	0.08 cm		Rib thickness	0.08	
Total flow area	3.653 cm <sup>2</sup>		Total flow area	7.827 cm <sup>2</sup>	
Flow velocity	15 m/sec		Flow velocity	7.0 m/sec	
Number of Channels	Channel Width, cm	Channel Depth, cm	Number of Channels	Channel Width, cm	Channel Depth, cm
80	0.257	0.177			
100	0.193	0.189	100	0.456	0.171
120	0.145	0.210	120	0.367	0.179
140	0.113	0.231	140	0.303	0.184
150	0.100	0.243	150	0.277	0.188
160	0.092	0.247	160	0.255	0.192
180	0.070	0.289	180	0.218	0.196

location along the thrust chamber profile. The number of channels or tubes will determine the shape of the cross section, ranging from deep and thin to almost square. The effect of varying the number of channels or channel dimensions and shape is shown in Table 8-6. The minimum inert mass of the cooling jacket and a low friction loss occur, when the shape (which varies axially throughout the jacket) is on the average close to a square. On the basis of analyses, as shown in the table, a 150-channel design has been selected for giving favorable cross section, reasonable dimensions for ease of fabrication, good cooling and often low thermal wall stresses.

Reinforcing bands have to be put on the outside of the tubes or channels to hold the internal gas pressure during operation, to contain the coolant pressures, which cause heated walls wanting to become round, and any surge pressures during the start transient or arising from water hammer in the lines. We assume a surge pressure of 50% above chamber pressure and a steel strength  $\sigma$  of 120,000 psi. In the chamber the inside diameter is 16.7 cm (6.57 in.), the walls and channels are 0.3 cm thick, and the pressure is 700 psia or 4.826 MPa. If one band allows the reinforcing of a length of chamber of 3.0 in. the cross sectional area of that reinforcing band will be  $A = pDL/(2\sigma) = [700 \times 1.5 \times (6.57 + 0.3) \times 3]/(2 \times 120,000) = 0.0902$  in. If the band were 1.0 in. wide, its thickness would be 0.09 in. and if it were 3 in. wide it would be 0.3 in. thick. Large nozzle exit sections have been observed to experience flutter or cyclic deformation, and therefore some stiffening rings may be needed near the exit.

The capacity of the fuel to absorb heat is approximately  $c_p m_f \Delta T = 0.5 \times 4.81 \times 200 = 278,000$  J/sec. The maximum  $\Delta T$  is established by keeping the

fuel well below its chemical decomposition point. This calculated heat absorption is less than the heat transfer from the hot gases. It is therefore necessary to reduce the gas temperature near the chamber and nozzle walls or to increase the heat absorption. This can be accomplished by (1) introducing film cooling by injection into the chamber just ahead of the nozzle, by (2) modifying the injection patterns, so that a cooler, fuel-rich thick internal boundary layer is formed, or (3) by allowing some nucleate boiling in the throat region. The analysis of these three methods is not given here. Item (2), supplementary cooling, is selected because it is easy to design and build, and can be based on extensive data of prior favorable experience. However it causes a small loss of performance (up to about 1% in specific impulse).

**Injector Design.** The injector pattern can be any one of the several types shown in Figs. 8-3 and 8-4. For this propellant combination we have used both doublets (like and unlike), and triplets in the USA, and the Russians have used multiple hollow double posts with swirling or rotation of the flow in the outer annulus. Based on good experience and demonstrated combustion stability with similar designs, we select a doublet self impinging type stream pattern and an injector design similar to Fig 8-4. The impinging streams form fans of liquid propellant, which break up into droplets. Oxidizer and fuel fans alternate radially. We could also use a platelet design, like Fig. 8-5.

The pressure drop across the injector is usually set at values between 15 and 25% of the chamber pressure, in part to obtain high injection velocities, which aid in atomization and droplet breakup. In turn this leads to more complete combustion (and thus better performance) and to stable combustion. We will use 20% or 140 psi or 0.965 MPa for the injector pressure drop. There is a small pressure loss in the injector passages. The injection velocities are found from Eqs. 8-1 and 8-5. The equation is solved for the area  $A$ , which is the cumulative cross-section area of all the injection holes of one of the propellants in the injector face.

With rounded and clean injection hole entrances the discharge coefficient will be about 0.80 as shown in Table 8-2. Solving for the cumulative injection hole area for the fuel and the oxidizer flow gives  $1.98 \text{ cm}^2$  for the fuel and  $4.098 \text{ cm}^2$  for the oxidizer. A typical hole diameter in this size of injector would be about 0.5 to 2.5 mm. We will use a hole size of 1.5 mm for the fuel holes (with 90% of the fuel flow) and 2.00 mm for the oxidizer hole size, resulting in 65 doublets of oxidizer holes and 50 doublets of fuel. By using a slightly smaller fuel injection hole diameter, we can match the number of 65 doublets as used with the oxidizer holes. These injection doublets will be arranged on the injector face in concentric patterns similar to Fig. 8-4. We may be able to obtain a slightly higher performance by going to smaller hole sizes and a large number of fuel and oxidizer holes. In addition there will be extra fuel holes on the periphery of the injector face to help in providing the cooler boundary layer, which is needed to reduce heat transfer. They will use 10% of the fuel flow and,

for a 0.5 mm hole diameter, the number of holes will be about 100. To make a good set of liquid fans, equal inclination angles of about  $25^\circ$  are used with the doublet impingements. See Fig. 8-7.

**Ignition.** A pyrotechnic (solid propellant) igniter will be used. It has to have enough energy and run long enough to provide the pressure and temperature in the thrust chamber for good ignition. Its diameter has to be small enough to be inserted through the throat, namely 8.0 cm maximum diameter and 10 to 15 cm long.

**Layout Drawings, Masses, Flows, and Pressure Drops.** We now have enough of the key design parameters of the selected thrust chamber, so a preliminary layout drawing can be made. Before this can be done well, we will need some analysis or estimates on the manifolds for fuel and oxidizer, valve mounting provisions and their locations, a nozzle closure during storage, a thrust structure, and possibly an actuator and gimbal mount, if gimbaling is required by the mission. A detailed layout or CAD (Computer Aided Design) image (not shown in this analysis) would allow a more accurate picture and a good determination of the mass of the thrust chamber and its center of gravity both with and without propellants.

Estimates of gas pressures, liquid pressures (or pressure drops) in the flow passages, injector, cooling jacket, and the valves are needed for the stress analysis, so that various wall thicknesses and component masses can be determined. Material properties will need to be obtained from references or tests. A few of these analyses and designs may actually change some of the data we selected or estimated early in this sample analysis and some of the calculated parameters may have to be re-analyzed and revised. Further changes in the thrust chamber design may become evident in the design of the engine, the tanks, or the interface with the vehicle. The methods, processes and fixtures for manufacturing and testing (and the number and types of tests) will have to be evaluated and the number of thrust chambers to be built has to be decided, before we can arrive at a reasonable manufacturing plan, a schedule and cost estimates.

## PROBLEMS

1. How much total heat per second can be absorbed in a thrust chamber with an inside wall surface area of  $0.200 \text{ m}^2$  if the coolant is liquid hydrogen and the coolant temperature does not exceed 145 K in the jacket? Coolant flow is 2 kg/sec. What is the average heat transfer rate per second per unit area? Use the data from Table 7-1 and the following:

Heat of vaporization near boiling point	446 kJ/kg
Thermal conductivity (gas at 21 K)	0.013 W/m-K
(gas at 194.75 K)	0.128 W/m-K
(gas at 273.15 K)	0.165 W/m-K

2. During a static test a certain steel thrust chamber is cooled by water. The following data are given:

Average water temperature	100°F
Thermal conductivity of water	$1.07 \times 10^{-4}$ Btu/sec-ft <sup>2</sup> -°F/ft
Gas temperature	4500°F
Viscosity of water	$2.5 \times 10^{-5}$ lbf-sec/ft <sup>2</sup>
Specific heat of water	1.0 Btu/lb-°F
Cooling passage dimensions	$\frac{1}{4} \times \frac{1}{2}$ in.
Water flow through passage	0.585 lb/sec
Thickness of inner wall	$\frac{1}{8}$ in.
Heat absorbed	1.3 Btu/in. <sup>2</sup> -sec
Thermal conductivity of wall material	26 Btu/hr-ft <sup>2</sup> -°F/ft

Determine (a) the film coefficient of the coolant; (b) the wall temperature on the coolant side; (c) the wall temperature on the gas side.

3. In the example of Problem 2 determine the water flow required to decrease the wall temperature on the gas side by 100°F. What is the percentage increase in coolant velocity? Assume that the various properties of the water and the average water temperature do not change.
4. Express the total temperature drop in Problem 2 in terms of the percentage temperature drops through the coolant film, the wall, and the gas film.
5. Determine the absolute and relative reduction in wall temperatures and heat transfer caused by applying insulation in a liquid-cooled rocket chamber with the following data:

Tube wall thickness	0.381 mm
Gas temperature	2760 K
Gas-side wall temperature	1260 K
Heat transfer rate	15 MW/m <sup>2</sup>
Liquid film coefficient	23 kW/m <sup>2</sup> -K
Wall material	Stainless steel AISI type 302

A 0.2 mm thick layer of insulating paint is applied on the gas side; the paint consists mostly of magnesia particles. The conductivity of this magnesia is 2.59 W/m<sup>2</sup>-K/m. The stainless steel has an average thermal conductivity of 140 Btu/hr-ft<sup>2</sup>-°F/in.

6. A small thruster has the following characteristics:

Propellants	Nitrogen tetroxide and monomethyl hydrazine
Injection individual hole size	Between 0.063 and 0.030 in.
Injection hole pattern	Unlike impinging doublet
Thrust chamber type	Ablative liner with a carbon-carbon nozzle throat insert
Specific gravities:	1.446 for oxidizer and 0.876 for fuel
Impingement point	0.25 in. from injector face
Direction of jet momentum	Parallel to chamber axis after impingement
$r = 1.65$ (fuel rich)	$(I_s)_{\text{actual}} = 251$ sec
$F = 300$ lbf	$t_b = 25$ sec
$p_1 = 250$ psi	$A_1/A_t = 3.0$
$(\Delta p)_{ij} = 50.0$ psi	$(C_d)_0 = (C_d)_f = 0.86$

Determine the number of oxidizer and fuel holes and their angles. Make a sketch to show the symmetric hole pattern and the feed passages in the injector. To protect the wall, the outermost holes should all be fuel holes.

7. A large, uncooled, uninsulated, low carbon steel thrust chamber burned out in the throat region during a test. The wall (0.375 in. thick) had melted and there were several holes. The test engineer said that he estimated the heat transfer to have been about 15 Btu/in.<sup>2</sup>. The chamber was repaired and you are responsible for the next test. Someone suggested that a series of water hoses be hooked up to spray plenty of water on the outside of the nozzle wall at the throat region during the next test to prolong the firing duration. The steel's melting point is estimated to be 2550°F. Because of the likely local variation in mixture ratio and possibly imperfect impingement, you anticipate some local gas regions that are oxidizer rich and could start the rapid oxidation of the steel. You therefore decide that 2250°F should be the maximum allowable inner wall temperature. Besides knowing the steel weight density (0.284 lbf/in.<sup>3</sup>), you have the following data for steel for the temperature range from ambient to 2250°F: the specific heat is 0.143 Btu/lbm-°F and the thermal conductivity is 260 Btu/hr-ft<sup>2</sup>-°F/in. Determine the approximate time for running the next test (without burnout) both with and without the water sprays. Justify any assumptions you make about the liquid film coefficient of the water flow. If the water spray seems to be worth while (getting at least 10% more burning time), make sketches with notes on how the mechanic should arrange for this water flow so it will be most effective.

8. The following conditions are given for a double-walled cooling jacket of a rocket thrust chamber assembly:

Rated chamber pressure	210 psi
Rated jacket pressure	290 psi
Chamber diameter	16.5 in.
Nozzle throat diameter	5.0 in.
Nozzle throat gas pressure	112 psi
Average inner wall temperature at throat region	110°F
Average inner wall temperature at chamber region	800°F
Cooling passage height at chamber and nozzle exit	0.375 in.
Cooling passage height at nozzle throat	0.250 in.
Nozzle exit gas pressure	14.7 psi.
Nozzle exit diameter	10 in.
Wall material	1020 carbon steel
Safety factor on yield strength	2.5
Cooling fluid	RP-1
Average thermal conductivity of steel	250 Btu/hr-ft <sup>2</sup> -F/in.

Assume other parameters, if needed. Compute the outside diameters and the thickness of the inner and outer walls at the chamber, at the throat, and at the nozzle exit.

9. Determine the hole sizes and the angle setting for a multiple-hole, doublet impinging stream injector that uses alcohol and liquid oxygen as propellants. The resultant momentum should be axial, and the angle between the oxygen and fuel jets ( $\gamma_o + \gamma_f$ ) should be 60°. Assume the following:

$(C_d)_o$	0.87	Chamber pressure	300 psi
$(C_d)_f$	0.91	Fuel pressure	400 psi

$\rho_o$	71 lb/ft <sup>3</sup>	Oxygen pressure	380 psi
$\rho_f$	51 lb/ft <sup>3</sup>	Number of jet pairs	4
$r$	1.20	Thrust	250 lbf
		Actual specific impulse	218 sec

Answers: 0.0197 in.; 0.0214 in.; 32.3°; 27.7°.

10. Explain in a rational manner why Fig. 8-10 has a maximum and how this maximum would be affected by the duty cycle, ablative material, heat loss from the thrust chamber, effect of altitude, and so on. Why does this maximum not occur at 90% burn time?
11. Table 10-5 shows that the RD 120 rocket engine can operate down to 85% of full thrust and at a mixture ratio variation of  $\pm 10.0\%$ . In a particular static test the average thrust was held at 96% of nominal and the average mixture ratio was 2.0% fuel rich. Assume a 1.0% residual propellant, but neglect other propellant budget allowances. What percentage of the fuel and oxidizer that have been loaded will remain unused at thrust termination? If we want to correct the mixture ratio in the last 20.0% of the test duration and use up all the available propellant, what would be the mixture ratio and propellant flows for this last period?
12. Make a simple sketch to scale of the thrust chamber that was analyzed in Section 8.6. The various dimensions should be close, but need not be accurate. Include or make separate sketches of the cooling jacket and the injector. Also compile a table of all the key characteristics, similar to Table 8-1, but include gas generator flows, and key materials. Make estimates or assumptions for any key data that is not mentioned in Section 8.6

## SYMBOLS

$A$	area, m <sup>2</sup> (ft <sup>2</sup> )
$A_a$	Projected area of linear aerospike ramp, m <sup>2</sup> (ft <sup>2</sup> )
$c_p$	specific heat at constant pressure, J/kg-K (Btu/lbm R)
$\bar{c}$	average liquid specific heat, J/kg-K (Btu/lbm R)
$C_d$	discharge coefficient
$C_F$	thrust coefficient (see Eq. 3-31)
$D$	diameter, m (ft)
$E$	modulus of elasticity, N/m <sup>2</sup> (lbf/in. <sup>2</sup> ), or radiation energy, kg-m <sup>2</sup> /sec <sup>2</sup>
$f$	friction loss coefficient, or geometric factor in radiation
$g_0$	sea level acceleration of gravity, 9.806 m/sec <sup>2</sup> (32.17 ft/sec <sup>2</sup> )
$h$	film coefficient, W/(m <sup>2</sup> -K)
$\Delta h$	enthalpy change, J/kg (Btu/lb)
$I_s$	specific impulse, sec
$k$	specific heat ratio
$L$	length, m (ft)
$L^*$	characteristic chamber length, m (ft)
$m$	mass, kg

$\dot{m}$	mass flow rate, kg/sec (lb/sec)
$p$	pressure, N/m <sup>2</sup> or Pa (lbf/in. <sup>2</sup> )
Pr	Prandtl number ( $c_p \mu / \kappa$ )
$q$	heat-transfer rate or heat flow per unit area, J/m <sup>2</sup> -sec (Btu/ft <sup>2</sup> -sec)
$Q$	volume flow rate, m <sup>3</sup> /sec (ft <sup>3</sup> /sec), or heat flow rate, J/sec
$r$	flow mixture ratio (oxidizer to fuel)
$s$	stress N/m <sup>2</sup> (lbf/in. <sup>2</sup> )
$t$	time, sec
$t_s$	stay time, sec
$t_w$	wall thickness, m (in.)
$T$	absolute temperature, K (R)
$v$	velocity, m/sec (ft/sec)
$\mathcal{V}$	specific volume, m <sup>3</sup> /kg(ft <sup>3</sup> /lb)
$V_c$	combustion chamber volume (volume up to throat), m <sup>3</sup> (ft <sup>3</sup> )

### Greek Letters

$\gamma_o$	angle between chamber axis and oxidizer stream
$\gamma_f$	angle between chamber axis and fuel stream
$\Delta$	finite differential
$\delta$	angle between chamber axis and the resultant stream
$\epsilon$	nozzle area ratio ( $\epsilon = A_2/A_1$ ), or emissivity of radiating body
$\theta$	angle
$\kappa$	thermal conductivity, J/(m <sup>2</sup> -sec-K)/m (Btu/in. <sup>2</sup> -sec <sup>2</sup> - R/in.)
$\lambda$	coefficient of thermal expansion, m/m-K (in./in.-R)
$\mu$	viscosity, m <sup>2</sup> /sec
$\nu$	Poisson ratio
$\rho$	density, kg/m <sup>3</sup> (lbf/ft <sup>3</sup> )
$\sigma$	Stefan-Boltzmann constant ( $5.67 \times 10^{-8}$ W/m <sup>2</sup> -K <sup>4</sup> )

### Subscripts

am	arithmetic mean
$c$	chamber
$f$	fuel or final condition
$g$	gas
$l$	liquid
$o$	oxidizer
$t$	throat
$w$	wall
$wg$	wall on side of gas
$wl$	wall on side of liquid
0	initial condition



- 1 inlet or chamber condition
- 2 nozzle exit condition
- 3 atmosphere or ambient condition

## REFERENCES

- 8-1. R. Sackheim, D. F. Fritz, and H. Maklis, "The Next Generation of Spacecraft Propulsion Systems," *AIAA Paper 79-1301*, 1979.
- 8-2. S. Peery and A. Minnick, "Design and Development of an Advanced Expander Combustor," *AIAA Paper 98-3675*, July 1998.
- 8-3. R. D. McKown, "Brazing the SSME," *Threshold, an Engineering Journal of Power Technology*, No. 1, Rocketdyne Division of Rockwell International (now The Boeing Co.), Canoga Park, CA, March 1987, pp. 8-13.
- 8-4. R. A. Ellis, J. C. Lee, F. M. Payne, M. Lacoste, A. Lacombe, and P. Joyes, "Testing of the RL10B-2 Carbon-Carbon Nozzle Extension," *AIAA Conference Paper 98-3363*, July 1998.
- 8-5. M. Niino, A. Kumakawa, T. Hirano, K. Sumiyashi, and R. Watanabe, "Life Prediction of CIP Formed Thrust Chambers," *Acta Astronautica*, Vol. 13, Nos. 6-7, 1986, pp. 363-369 (fatigue life prediction).
- 8-6. J. S. Porowski, W. J. O'Donnell, M. L. Badlani, B. Kasraie, and H. J. Kasper, "Simplified Design and Life Predictions of Rocket Thrustchambers," *Journal of Spacecraft and Rockets*, Vol. 22, No. 2, March-April 1985, pp. 181-187.
- 8-7. J. S. Kinkaid, "Aerospike Evolution," *Threshold*, The Boeing Co., Rocketdyne Propulsion and Power, No. 18, Spring 2000, pp. 4-13.
- 8-8. T. Harmon, "X-33 Linear Aerospike on the Fast Track in System Engineering," *AIAA Paper 99-2181, Joint Propulsion Conference*, June 1999.
- 8-9. A. J. Fortini and R. H. Tuffias, "Advanced Materials for Chemical Propulsion: Oxide-Iridium/Rhenium Combustion Chambers," *AIAA Paper 99-2894*, June 1999.
- 8-10. F. P. Incropera and D. P. DeWitt, *Introduction to Heat Transfer*, John Wiley & Sons, New York, 1996.
- 8-11. A. A. Samarskii and P. N. Vabishchevich, *Computational Heat Transfer, Vol. 1. Mathematical Modeling and Vol. 2. The Finite Difference Methodology*, John Wiley & Sons, New York, 1995.
- 8-12. D. R. Bartz, "Survey of Relationships between Theory and Experiment for Convective Heat Transfer in Rocket Combustion Gases," in *Advances in Rocket Propulsion*, S. S. Penner (Ed.), AGARD, Technivision Services, Manchester, UK, 1968.
- 8-13. N. Sugathan, K. Srinivathan, and S. Srinivasa Murthy, "Experiments on Heat Transfer in a Cryogenic Engine Thrust Chamber," *Journal of Propulsion and Power*, Vol. 9, No. 2, March-April 1993.
- 8-14. E. Mayer, "Analysis of Pressure Feasibility Limits in Regenerative Cooling of Combustion Chambers for Large Thrust Rockets," in *Liquid Rockets and*

- Propellants*, L. E. Bollinger, M. Goldsmith, and A. W. Lemmon, Jr (Eds.), Academic Press, New York, 1969, pp. 543–561.
- 8–15. J. M. Fowler and C. F. Warner, “Measurements of the Heat-Transfer Coefficients for Hydrogen Flowing in a Heated Tube,” *American Rocket Society Journal*, Vol. 30, No. 3, March 1960, pp. 266–267.
- 8–16. P.-A. Baudart, V. Duthoit, T. Delaporte, and E. Znaty, “Numerical Modeling of the HM 7 B Main Chamber Ignition,” *AIAA Paper 89-2397*, 1989.
- 8–17. A. R. Casillas, J. Eninger, G. Josephs, J. Kenney, and M. Trinidad, “Control of Propellant Lead/Lag to the LEA in the AXAF Propulsion System,” *AIAA Paper 98-3204*, July 1998.